

Event-by-event jet anisotropy and hard-soft tomography of the quark-gluon plasma

Yayun He,^{1,2,3} Wei Chen,⁴ Tan Luo,⁵ Shanshan Cao,^{6,*} Long-Gang Pang,^{1,†} and Xin-Nian Wang^{1,7,‡}

¹*Key Laboratory of Quark and Lepton Physics (MOE) and Institute of Particle Physics,
Central China Normal University, Wuhan 430079, China*

²*Guangdong Provincial Key Laboratory of Nuclear Science, Institute of Quantum Matter,
South China Normal University, Guangzhou 510006, China*

³*Guangdong-Hong Kong Joint Laboratory of Quantum Matter,
Southern Nuclear Science Computing Center, South China Normal University, Guangzhou 510006, China*

⁴*School of Nuclear Science and Technology, University of Chinese Academy of Sciences, Beijing 100049, China*

⁵*Instituto Galego de Física de Altas Enerxías IGFAE,
Universidade de Santiago de Compostela, E-15782 Galicia-Spain*

⁶*Institute of Frontier and Interdisciplinary Science,
Shandong University, Qingdao, Shandong 266237, China*

⁷*Nuclear Science Division Mailstop 70R0319, Lawrence Berkeley National Laboratory, Berkeley, California 94720[§]*

Suppression of jet spectra or jet quenching in high-energy heavy-ion collisions is caused by jet energy loss in the dense medium. The azimuthal anisotropy of jet energy loss in non-central heavy-ion collisions can lead to jet anisotropy which in turn can provide insight into the path-length dependence of jet quenching. This is investigated within the Linear Boltzmann Transport (LBT) model which simulates both elastic scattering and medium-induced gluon radiation based on perturbative QCD for jet shower and medium recoil partons as well as radiated gluons as they propagate through the quark-gluon plasma (QGP). The dynamical evolution of the QGP in each event of heavy-ion collisions is provided by the (3+1)D CLVisc hydrodynamic model with fully fluctuating initial conditions. This framework has been shown to describe the suppression of single inclusive jet spectra well. We calculate in this study the elliptic (v_2^{jet}) and triangular (v_3^{jet}) anisotropy coefficients of the single inclusive jet spectra in Pb+Pb collisions at the LHC energies. We investigate the colliding energy, centrality, jet transverse momentum dependence of the jet anisotropy, as well as their event-by-event correlation with the flow coefficients of the soft bulk hadrons. An approximate linear correlation between jet and bulk v_2 is found. Effect of the bulk v_n fluctuation on v_n^{jet} is found negligible. The jet-induced medium excitation, which is influenced by radial flow, is shown to enhance v_2^{jet} and the enhancement increases with the jet cone size. The jet elliptic anisotropy v_2^{jet} is also found to be slightly enhanced by the shear viscosity of the bulk medium in comparison to the LBT results when jets propagate through an ideal hydrodynamic QGP medium.

I. INTRODUCTION

Jet quenching or the suppression of energetic particles from hard processes has been very successful in probing properties of the hot and dense matter called quark-gluon plasma (QGP) created in heavy-ion collisions. This phenomenon is caused by energy loss and transverse momentum broadening of a propagating parton due to multiple scattering and induced gluon bremsstrahlung when it traverses the dense medium [1–7]. Within perturbative QCD (pQCD), one can calculate the parton energy loss and transverse momentum broadening [8–14]. They are found to be directly proportional to the jet transport coefficient \hat{q} which is defined as the transverse momentum broadening squared per unit length of propagation and can be related to the local gluon density distribution of the medium [15–17]. Experimental measurements of jet quenching and phenomenological extraction of the jet transport coefficient can provide some of the important

properties of QGP [18–22].

Given the jet transport coefficient, the total transverse momentum broadening squared of a parton will be proportional to the total length of the propagation. The total radiative energy loss is, however, proportional to the length squared due to the non-Abelian Landau-Pomeranchuk-Migdal interference in the gluon bremsstrahlung induced by multiple scattering inside the medium [8, 9]. This unique length dependence of the radiative parton energy loss in pQCD will give rise to a unique system size dependence of the jet quenching phenomenon in high-energy heavy-ion collisions. In non-central heavy-ion collisions, the averaged path-length and total parton energy loss will depend on the azimuthal angle of the jet propagation relative to the reaction plane. Such an azimuthal angle dependence of the total energy loss was predicted [23] to give rise to the azimuthal angle dependence or azimuthal anisotropy of high transverse momentum jet and hadron spectra in non-central heavy-ion collisions which is very similar to the anisotropy of soft hadrons generated by the collective expansion and flow of the dense medium [24]. The study of jet azimuthal anisotropy therefore will provide us additional information about jet propagation, the geometrical and dynamic properties of the dense medium in heavy-ion collisions.

* shanshan.cao@sdu.edu.cn

† lgpang@mail.ccnu.edu.cn

‡ xnwang@lbl.gov

§ current address

Because of the rapid decrease of gluon number density or the local jet transport coefficient with time due to longitudinal and transverse expansion, the azimuthal anisotropy of the averaged total parton energy loss and the final hadron spectra are reduced [25, 26] from that of a simple 1-dimensional Bjorken system [23, 27]. The observed v_2 of charged hadrons at large transverse momentum p_T is larger than simple jet quenching model calculations that take into account of the geometry and hydrodynamic expansion of the dense medium in non-central heavy-ion collisions, especially at intermediate $p_T \sim 4$ -10 GeV/ c . The hadron anisotropy below $p_T < 2$ GeV/ c is shown to come mostly from collective flow of the dense medium and can be described well by viscous hydrodynamic models [28–31]. Simultaneous description of single inclusive hadron suppression and anisotropies have been shown to provide stronger constraint on jet transport dynamics, initial state of the QGP and the event-by-event fluctuation of the bulk medium [32–36]. Some exotic mechanisms such as interaction through magnetic monopoles in QCD [37–39] and a singular behavior of the temperature dependence of the jet transport coefficient near the QCD phase transition have also been proposed to resolve the v_2 puzzle. However, it is quite likely that a mundane physics mechanism could be the culprit. It is known that recombination of jet shower and medium partons can lead to enhancement of protons and kaons and their anisotropic flow in intermediate p_T in heavy-ion collisions [40–46] as well as in p+A collisions [47, 48]. Such a mechanism can also provide a consistent description of the suppression and v_2 of the single inclusive hadron spectra in the intermediate p_T . Indeed, parton energy loss and recombination in the hadronization can describe well both the suppression factor and v_2 of charmed D and beauty B mesons [49–51] as well as the light hadrons in heavy-ion collisions [52].

Since jets are reconstructed from clusters of hadrons within a given jet-cone, their energies are directly related to the parton energies before hadronization. They are less likely influenced by the non-perturbative hadronization processes which only contribute to the jet energy about 1 GeV within a cone-size of $R = 1$ [53]. The jet suppression and jet anisotropy can therefore be directly related to parton transport, geometry and dynamical evolution of the QGP in heavy-ion collisions. This will be the focus of our study in this paper. We will employ the Linear Boltzmann Transport (LBT) model [54–56] together with the (3+1)-dimensional CCNU (Central China Normal University) - LBNL (Lawrence Berkeley National Laboratory) viscous (CLVisc) hydrodynamic model [57–59] for bulk medium evolution to investigate event-by-event jet anisotropy in Pb+Pb collisions at the Large Hadron Collider (LHC) energies. In particular, we will study the correlation between anisotropies of hard jets and soft bulk hadrons, effects of the event-by-event fluctuation of the bulk hadron spectra, jet-induced medium response and viscosity of the bulk medium. The same framework has been shown to describe the suppression

of single inclusive jet spectra [60] as well as γ/Z -jet correlation [61, 62] in Pb+Pb collisions at the LHC energies.

The remainder of this paper will be organized as follows. We will start with a brief review of the LBT model for jet transport in Sec. II and the CLVisc hydrodynamic model for the bulk evolution in Sec. III. After that, we will present and discuss our results on the elliptic flow coefficient (v_2) of single inclusive jets in Sec. IV and triangular flow coefficient (v_3) in Sec. V. In Sec. VI, effects of jet-induced medium response on jet anisotropic coefficients and their dependence on the jet-cone size will be explored in detail. The effect of the viscosity of the bulk medium on the final jet elliptic anisotropy v_2 will be discussed in Sec. VII. A summary will be given in Sec. VIII.

II. THE LINEAR BOLTZMANN TRANSPORT MODEL

The LBT model is based on the Boltzmann transport equation that includes both elastic and inelastic scatterings of jet shower partons as well as recoil medium partons inside the QGP medium [54–56]:

$$p_a \cdot \partial f_a = \int \sum_{bcd} \prod_{i=b,c,d} \frac{d^3 p_i}{2E_i (2\pi)^3} (f_c f_d - f_a f_b) |\mathcal{M}_{ab \rightarrow cd}|^2 \times \frac{\gamma_b}{2} S_2(\hat{s}, \hat{t}, \hat{u}) (2\pi)^4 \delta^4(p_a + p_b - p_c - p_d) + \text{inelastic}, \quad (1)$$

where p_i ($i = a, b, c, d$) is the four momentum of parton i whose phase-space distribution function is $f_i = (2\pi)^3 \delta^3(\vec{p} - \vec{p}_i) \delta^3(\vec{x} - \vec{x}_i - \vec{v}_i t)$ for jet shower and recoil partons ($i = a, c$), and $f_i = 1/(e^{p_i \cdot u/T} \pm 1)$ for thermal medium partons ($i = b, d$) that are assumed in local equilibrium with temperature T and flow velocity u and “+ (−)” for quarks (gluons). Note that this equation includes both a gain term ($f_c f_d$) and a loss term ($-f_a f_b$). Here, the quantum effects of Pauli exclusion and Bose enhancement in the transport equation are assumed small and neglected. The summation over b, c and d takes into account all possible elastic processes $a + b \rightarrow c + d$ in which the scattering amplitude $|\mathcal{M}_{ab \rightarrow cd}|$ is calculated in the leading-order pQCD. The factor γ_b represents the color and spin degeneracy of parton b . To regularize the collinear divergence in the scattering amplitude, a Lorentz-invariant double-step function is adopted as follows,

$$S_2(\hat{s}, \hat{t}, \hat{u}) = \theta(\hat{s} \geq 2\mu_D^2) \theta(-\hat{s} + \mu_D^2 \leq \hat{t} \leq -\mu_D^2), \quad (2)$$

where \hat{s} , \hat{t} , and \hat{u} are the Mandelstam variables, and $\mu_D^2 = \frac{3}{2} g^2 T^2$ is the Debye screening mass taking into account both quark (three light flavors) and gluon degrees of freedom. A fixed strong coupling constant $\alpha_s = g^2/4\pi$ is used in the present work, which is tuned to describe experimental data on single inclusive jet spectra.

The inelastic part in Eq. (1) includes gluon radiation induced by the elastic scattering processes discussed

above. The induced gluon emission rate Γ_a^{inel} is taken from the higher-twist calculation [13, 63–65],

$$\frac{d\Gamma_a^{\text{inel}}}{dzdk_\perp^2} = \frac{6\alpha_s P_a(z)k_\perp^4}{\pi(k_\perp^2 + z^2m^2)^4} \frac{p \cdot u}{p_0} \hat{q}_a(x) \sin^2 \frac{\tau - \tau_i}{2\tau_f}, \quad (3)$$

where $P_a(z)$ is the splitting function for parton a (with mass m) to radiate a gluon with energy fraction z and transverse momentum k_\perp . The infrared divergence of the splitting function is also regularized by the Debye screening mass μ_D as the lower cut-off energy of the radiated gluon. In the sine term, $\tau_f = 2p_0z(1-z)/(k_\perp^2 + z^2m^2)$ is the formation time of the emitted gluon, and τ_i is the production time of the present parton, i.e., the time of the previous gluon emission. The jet transport coefficient $\hat{q}_a(x)$ represents the transverse momentum transfer squared per unit length/time due to elastic scatterings and is evaluated in the local comoving frame of the QGP medium as

$$\hat{q}_a(x) = \sum_{bcd} \rho_b(x) \int d\hat{t} q_\perp^2 \frac{d\sigma_{ab \rightarrow cd}}{d\hat{t}}, \quad (4)$$

where $\rho_b(x)$ is the parton density with the color and spin degeneracy included.

Given the elastic and inelastic scattering rates

$$\Gamma_a^{\text{el}} = \frac{p \cdot u}{p_0} \sum_{bcd} \rho_b(x) \sigma_{ab \rightarrow cd}, \quad (5)$$

$$\Gamma_a^{\text{inel}} = \frac{1}{1 + \delta_g^a} \int dz dk_\perp^2 \frac{d\Gamma_a^{\text{inel}}}{dz dk_\perp^2}, \quad (6)$$

from Eqs. (1) and (3), the elastic and inelastic scattering probabilities of parton a within a time step $\Delta\tau$ in the LBT simulations are calculated as

$$P_{\text{el}}^a = 1 - \exp[-\Delta\tau \Gamma_a^{\text{el}}(x)] \quad (7)$$

and

$$P_{\text{inel}}^a = 1 - \exp[-\Delta\tau \Gamma_a^{\text{inel}}(x)] \quad (8)$$

respectively, where we assume the numbers of both elastic and inelastic scatterings during $\Delta\tau$ obey Poisson distributions, whose average values are $\Delta\tau \Gamma_a^{\text{el}}$ and $\Delta\tau \Gamma_a^{\text{inel}}$, respectively. The latter may also be interpreted as the average number of emitted gluons $\langle N_g^a \rangle$ during this time interval. Therefore, Eq. (7) / (8) gives the probability for at least one elastic/inelastic scattering during this time interval $\Delta\tau$.

The total scattering probability is given by

$$P_{\text{tot}}^a = P_{\text{el}}^a(1 - P_{\text{inel}}^a) + P_{\text{inel}}^a, \quad (9)$$

where the first term on the right-hand side is for pure elastic processes without induced gluon emission, and the second term is for inelastic processes with at least one gluon emission. Based on the total probability, we first

decide whether a given parton scatters with the QGP during this $\Delta\tau$. If it scatters, the ratio between these two terms is used to determine whether the scattering is pure elastic or inelastic. In either case, an elastic scattering will be sampled first, whose specific channel is determined using the branching ratio $\Gamma_{a+b \rightarrow c+d}^{\text{el}}/\Gamma_a^{\text{el}}$. With a selected channel, the energies and momenta of partons b , c and d are then sampled with the differential rate given by the first part of Eq. (1). In case of inelastic scattering, the number of emitted gluons n will be first decided according to a Poisson distribution with the mean value $\langle N_g^a \rangle$. The energy-momentum of each gluon is then sampled with the spectra given by Eq. (3). In the end, the energies and momenta of these n gluons will be adjusted together with those of c and d such that the $2 \rightarrow 2 + n$ process respects the energy-momentum conservation.

In the LBT model, we track all partons involved in the scatterings. We define c or d with a larger energy as the jet shower parton, while the other as the recoil parton. Medium induced gluons are also tracked as jet shower partons. Parton b which is scattered out of the thermal medium background is denoted as a “negative” parton from the back-reaction and is allowed to go through further scattering in LBT. It is essentially a particle hole left in the medium when the original thermal parton is scattered out. Thus, its four-momentum will be subtracted from the reconstructed jets in our analysis of simulated events from LBT. Both recoil and “negative” (back-reaction) partons are considered as jet-induced medium excitation, or medium response to jet propagation, whose importance has been verified in many jet observables within the LBT model [60, 61].

The term “linear” in LBT denotes a linear approximation adopted in this model, where we only consider jet/recoil/“negative” parton interaction with the medium, but not among themselves, assuming their number density negligible compared to the thermal partons inside the QGP. A full calculation that includes such non-linear interactions can be realized within a coupled LBT-hydrodynamic (CoLBT-hydro) model that has been developed in Refs. [66–68]. Such a coupled approach is important to describing properties of the jet-induced medium response in detail. But the effect of interaction among recoil and soft radiated gluons beyond the linear approximation is negligible on the energy of reconstructed jets and the final jet spectra.

III. CLVISC HYDRODYNAMICS FOR BULK MEDIUM EVOLUTION

To take into account the evolution of the QGP in heavy-ion collisions in the LBT model, we use the space-time profile of the bulk medium from the CLVisc (3+1)D viscous hydrodynamic model [57–59]. CLVisc parallelizes Kurganov-Tadmor algorithm [69] to solve the hydrodynamic equation for the bulk medium and Cooper-Frye particlization on GPU, using Open Computing Language

(OpenCL). Parallelized with massive amount of processing elements on GPUs and Single Instruction Multiple Data (SIMD) vector operations on modern CPUs, CLVisc brings about the best performance increase so far to (3+1)D hydrodynamics on heterogeneous computing devices and provides the event-by-event space-time hydrodynamic profiles for simulations of jet transport within LBT model in this study.

The dynamical evolution of the locally thermalized system in heavy-ion collisions is described by relativistic hydrodynamic equations,

$$\nabla_\mu T^{\mu\nu} = 0, \quad (10)$$

where ∇_μ is the covariant derivative operator, $T^{\mu\nu} = (\epsilon + P)u^\mu u^\nu - Pg^{\mu\nu} + \pi^{\mu\nu}$ is the energy-momentum stress tensor, in which ϵ and P are the energy density and pressure in the co-moving frame of the fluid, u^μ is the relativistic fluid four-velocity, $g^{\mu\nu} = \text{diag}(1, -1, -1, -1)$ is the metric tensor in the Milne (τ, x, y, η_s) coordinates and $\pi^{\mu\nu}$ is the shear-stress tensor which will depend on the bulk transport coefficients. In the case of an ideal hydrodynamics, this term is set to zero. To solve this group of time-dependent partial differential equations, one needs the energy-momentum tensor $T^{\mu\nu}$ at the initial time τ_0 and the equation of state (EoS) $P = P(\epsilon)$.

The initial condition for the energy-momentum density distributions for event-by-event CLVisc hydrodynamic simulations in this study are obtained from A Multi-Phase Transport (AMPT) model [58, 70] with a Gaussian smearing,

$$T^{\mu\nu}(\tau_0, x, y, \eta_s) = K \sum_i \frac{p_i^\mu p_i^\nu}{p_i^\tau} \frac{1}{\tau_0 \sqrt{2\pi\sigma_{\eta_s}^2}} \frac{1}{2\pi\sigma_r^2} \times \exp \left[-\frac{(x - x_i)^2 + (y - y_i)^2}{2\sigma_r^2} - \frac{(\eta_s - \eta_{is})^2}{2\sigma_{\eta_s}^2} \right], \quad (11)$$

where $p_i^\tau = m_{iT} \cosh(Y_i - \eta_{is})$ and $p_i^\eta = m_{iT} \sinh(Y_i - \eta_{is})/\tau_0$ with $m_{iT} = \sqrt{p_{ix}^2 + p_{iy}^2 + m^2}$. The summation runs over all partons (i) produced in the AMPT model simulations. We have chosen $\sigma_r = 0.6$ fm and $\sigma_{\eta_s} = 0.6$ in our calculations which provide a reasonable description of soft hadron observables [59]. The transverse mass m_T , rapidity Y and spatial rapidity η_s are calculated from parton's 4-momenta and spatial coordinates. Note that there is no Bjorken scaling in the above initial condition because of early parton cascade in AMPT model. The scale factor K and the initial time τ_0 are two parameters that can be adjusted to fit the experimental data on the central rapidity density of produced hadrons.

For most calculations in this study, we use the ideal version of CLVisc with a parametrized equation of state (EoS) s95p-v1 [71] to obtain the hydrodynamic evolution of the bulk medium. We will discuss the effect of shear viscosity on jet quenching and anisotropy at the end of this paper. In each centrality bin, we simulate 200 events of hydrodynamic evolution of the dense medium in

$\langle v_2^{\text{soft}} \rangle \pm \delta v_2^{\text{soft}}$		
	2.76 TeV	5.02 TeV
5 – 10%	0.047 ± 0.007	0.054 ± 0.008
10 – 20%	0.060 ± 0.008	0.076 ± 0.007
20 – 30%	0.076 ± 0.008	0.086 ± 0.008
30 – 40%	0.089 ± 0.008	0.095 ± 0.009
40 – 50%	0.079 ± 0.008	0.086 ± 0.009
50 – 60%	0.078 ± 0.009	0.078 ± 0.009

TABLE I. The mean values and standard deviations of soft hadron v_2^{soft} in Pb+Pb collisions at $\sqrt{s} = 2.76$ TeV and 5.02 TeV in centrality bins 5 – 10%, 10 – 20%, 20 – 30%, 30 – 40%, 40 – 50% and 50 – 60% from the CLVisc model.

$\langle v_3^{\text{soft}} \rangle \pm \delta v_3^{\text{soft}}$		
	2.76 TeV	5.02 TeV
5 – 10%	0.031 ± 0.007	0.027 ± 0.007
10 – 20%	0.031 ± 0.007	0.029 ± 0.007
20 – 30%	0.032 ± 0.007	0.035 ± 0.008
30 – 40%	0.034 ± 0.007	0.035 ± 0.008
40 – 50%	0.038 ± 0.007	0.034 ± 0.008
50 – 60%	0.035 ± 0.007	0.032 ± 0.008

TABLE II. The mean value and standard deviation of soft hadron v_3^{soft} in Pb+Pb collisions at $\sqrt{s} = 2.76$ TeV and 5.02 TeV in centrality bins 5 – 10%, 10 – 20%, 20 – 30%, 30 – 40%, 40 – 50% and 50 – 60% from the CLVisc model.

heavy-ion collisions in order to include the effect of event-by-event fluctuations on jet transport. To improve the statistics of high- p_T jets, we divide the initial transverse momentum transfer p_{Ti} in PYTHIA 8 simulations into multiple bins and generate 10000 sets of initial jet showers from PYTHIA 8 in each p_{Ti} bin for each of the above-mentioned hydrodynamic profile. The total number of jet events for each p_{Ti} bin is therefore $N_{\text{event}} = 200 \times 10000$ for each centrality bin under investigation. This is also the total number of events we use for simulating $p + p$ collisions in each p_{Ti} bin for the calculation of the single inclusive jet suppression factor [60]. The jet cross sections in different p_{Ti} bins of initial hard scatterings will be used as weights in calculating the final jet spectra in both $p + p$ and A+A collisions.

For the spatial distribution of the initial jet production vertices, we also use the AMPT model that employs the HIJING model [72, 73] to generate minijets according to the Glauber model of nuclear collisions with the Woods-Saxon nuclear distribution. The geometrical distribution of the initial jets in the transverse plane in each p_{Ti} bin is sampled according to this initial minijet distribution in each AMPT event, as shown in Fig. 1. The same AMPT event also provides the initial condition for the energy-momentum density distribution for the CLVisc hydrodynamic simulation of the space-time evolution of the bulk medium. The centrality classes of heavy-ion collisions are defined according to the initial parton multiplicity distribution, and the averaged number of participant nucleons $\langle N_{\text{part}} \rangle$ in each centrality class is computed accordingly.

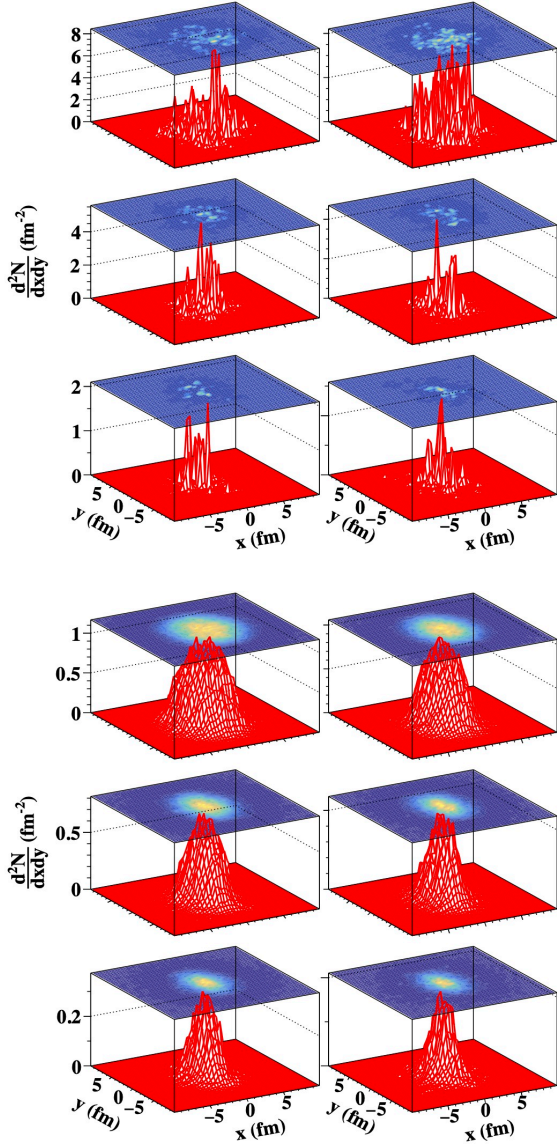


FIG. 1. (Color online) Distributions of initial jet production positions in the transverse plane of Pb+Pb collisions at $\sqrt{s} = 5.02$ TeV in the centrality bins 5 – 10%, 10 – 20%, 20 – 30%, 30 – 40%, 40 – 50% and 50 – 60% (from left to right and top to bottom) for one hydrodynamic event (upper panel) and averaged over 200 hydrodynamic events (lower panel).

To demonstrate the event-by-event fluctuation of the bulk medium, we present the distributions of the elliptic and triangular flow coefficients of the final bulk hadrons from our event-by-event hydrodynamic calculations in Figs. 2 and 3. Results for Pb+Pb collisions at both $\sqrt{s} = 2.76$ TeV and 5.02 TeV are shown, and compared to available data in different centrality bins from ATLAS [74] and CMS experiments [75]. A reasonable agreement between our hydrodynamic simulations and the experimental data is achieved except at very large values of v_2^{soft} and v_3^{soft} where statistics of the hydrodynamic simu-

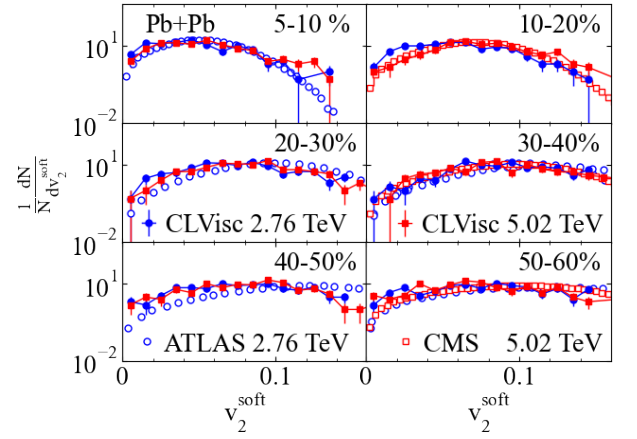


FIG. 2. (Color online) Distributions of soft hadron v_2^{soft} from 200 hydro events calculated with CLVisc model in Pb+Pb collisions at $\sqrt{s} = 2.76$ TeV (closed blue circle) and 5.02 TeV (closed red square) in each centrality bin 5 – 10%, 10 – 20%, 20 – 30%, 30 – 40%, 40 – 50% and 50 – 60% as compared to data from the ATLAS experiments in Pb+Pb collisions at $\sqrt{s} = 2.76$ TeV (open blue circle) in centrality bins 5 – 10%, 20 – 25%, 30 – 35%, 40 – 45%, 55 – 60% [74] and the CMS experiment at $\sqrt{s} = 5.02$ TeV (open red square) in centrality bins 15 – 20%, 30 – 35%, 55 – 60% [75].

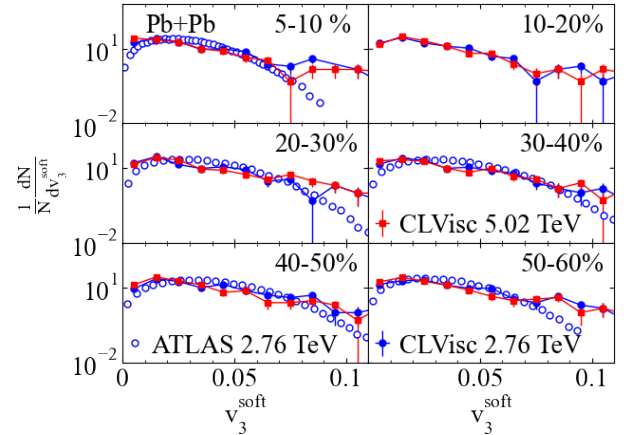


FIG. 3. (Color online) Distributions of soft hadron v_3^{soft} from 200 hydro events calculated with CLVisc model in Pb+Pb collisions at $\sqrt{s} = 2.76$ TeV (closed blue circle) and 5.02 TeV (closed red square) in centrality bin 5 – 10%, 10 – 20%, 20 – 30%, 30 – 40%, 40 – 50% and 50 – 60% as compared to the ATLAS experimental data at Pb+Pb $\sqrt{s} = 2.76$ TeV (open blue circle) in centrality bins 5 – 10%, 20 – 25%, 30 – 35%, 40 – 45%, 55 – 60% [74].

lations becomes very limited. To quantify these v_n^{soft} distributions, we summarize the average values of v_2^{soft} and v_3^{soft} in Tabs. I and II, respectively, together with their corresponding fluctuations δv_2^{soft} and δv_3^{soft} for different centrality bins and colliding energies. One may observe from Tab. I that $\langle v_2^{\text{soft}} \rangle$ first increases and then decreases as centrality increases. Within a given centrality bin, $\langle v_2^{\text{soft}} \rangle$ in Pb+Pb collisions at $\sqrt{s} = 5.02$ TeV is larger

than that at 2.76 TeV, except in very peripheral collisions. The event-by-event fluctuation of the elliptic flow $\delta v_2^{\text{soft}}/v_2^{\text{soft}}$ is around 10%~15%. In contrast, as shown in Tab. II, the bulk $\langle v_3^{\text{soft}} \rangle$ has a quite weak dependence on centrality and colliding system under discussion, because it is mainly driven by event-by-event fluctuation instead of the average geometry of the bulk medium. The value of $\delta v_3^{\text{soft}}/v_3^{\text{soft}}$ is around 20%~25%.

IV. SINGLE INCLUSIVE JET ANISOTROPY v_2^{jet}

A. LBT simulations and analyses

To calculate jet spectra in realistic heavy-ion collisions, we first use PYTHIA 8 to generate initial jet shower partons in $p + p$ collisions at the corresponding colliding energy. In order to obtain sufficient statistics for our final results, we divide the (0, 350) GeV/ c range of the transverse momentum transfer for the initial hard scatterings into seven equal bins, each with the width of 50 GeV/ c . In each of these triggering p_T bins, 2 million events are simulated in total, with 10000 events in which jet shower partons propagate through each of the 200 hydrodynamic profiles that we obtain via the CLVisc model as discussed in the previous section. Using 200 hydrodynamic profiles per centrality bin allows one to take into account of the effects of the event-by-event fluctuations in the bulk medium on the final jet observables. The initial position of each jet production is sampled according to the distribution of hard scattering locations in the AMPT model for each of the hydro event, which we consistently use to determine the initial condition of the bulk evolution. In this work, we only consider the distribution of the transverse locations of these jet production points, while neglect their spread in the longitudinal direction around the highly Lorentz contracted disc of two overlapping nuclei at high colliding energies.

The formation time of each jet shower parton is set as $p_T^2/2E$ with p_T and E being its initial transverse momentum and energy, respectively. The parton is assumed to stream freely before its formation time is reached. After this formation time, as well as the starting time of the hydrodynamic evolution ($\tau_0 = 0.6$ fm), whichever comes later, we simulate the interaction between jet shower partons and the hydrodynamic medium using the LBT model. After jet partons exit the QGP medium, we neglect their interactions with the hadron gas in this work, considering that the gluon density in the hadronic gas is much lower and the effective jet transport coefficient \hat{q} in a confined medium is much smaller [18] than that in the QGP medium.

In simulations of both $p + p$ and A+A collisions, we pass all final state partons to the FASTJET package [76] to reconstruct jets using the anti- k_T algorithm with a given jet-cone size R . The FASTJET package used in this study has been modified such that the energy-momentum of the “negative” partons from the LBT model is sub-

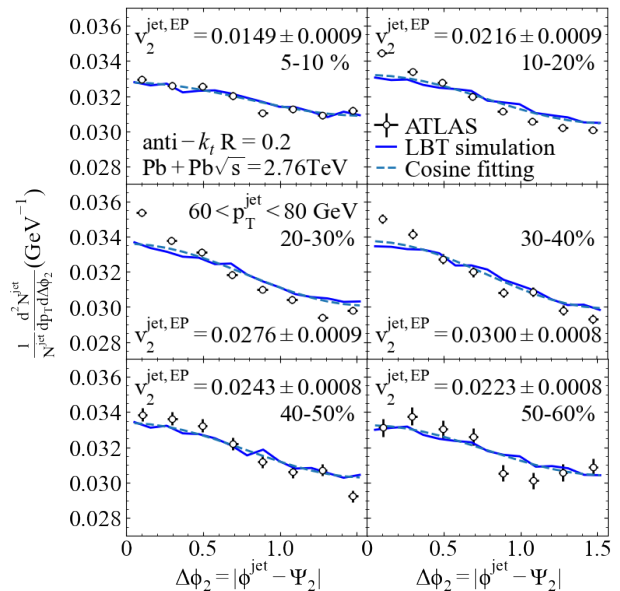


FIG. 4. (Color online) Distributions of the difference of the jet azimuthal angle ϕ^{jet} and the event plane angle Ψ_2 ($\Delta\phi_2 = \phi^{\text{jet}} - \Psi_2$) in different centrality bins of Pb+Pb collisions at $\sqrt{s} = 2.76$ TeV. Results calculated from the LBT model (blue solid lines) are compared to the ATLAS data [78] (black open circle) and fitted with a cosine function (blue dash lines).

tracted from jets in the reconstruction. When reconstructing jets via FASTJET, we also subtract the underlying event (UE) background using the scheme applied in experimental studies [77]. One may first define the seed jet as a jet with at least one particle whose transverse energy is higher than 3 GeV, and with a leading particle whose transverse energy is more than four times of the average value per particle within the jet. Then the transverse energy density of the UE background is calculated over the whole area under investigation excluding these seed jets. In the end, this UE transverse energy within the transverse area of each jet is subtracted from the jet energy in both $p + p$ and A+A collisions. In LBT simulations, we only consider evolution of jet shower partons, recoil partons and “negative” (back-reaction) partons, i.e., partons that directly participate in jet-medium interaction. Medium constituents that do not participate in this interaction are excluded for jet reconstruction. Therefore, the UE background in our analysis is very small compared to that in experimental analyses which also include soft hadrons from the QGP that are not directly correlated with the jet. Within this framework, we have verified in Ref. [60] that the jet spectra we obtain for $p + p$ collisions are consistent with the experimental data. With a fixed effective strong coupling constant $\alpha_s = 0.15$, LBT model provides a good description of the jet suppression factor R_{AA} in A+A collisions [60]. It provides a reliable baseline for our further investigation of the azimuthal anisotropy of jets in the present work.

B. Centrality dependence

To extract the anisotropic flow coefficient of the single inclusive jet spectra in A+A collisions, we express their normalized azimuthal distribution as,

$$\frac{1}{N^{\text{jet}}} \frac{dN^{\text{jet}}}{d\Delta\phi_n} \propto 1 + 2v_n^{\text{jet,EP}} \cos(n\Delta\phi_n), \quad (12)$$

where $\Delta\phi_n = \phi^{\text{jet}} - \Psi_n$ is the difference between the azimuthal angle of jets ϕ^{jet} and the n^{th} -order event plane angle Ψ_n , with Ψ_n being defined via $\langle e^{in\phi^{\text{soft}}} \rangle = v_n^{\text{soft}} e^{in\Psi_n}$ for each hydrodynamic event. The superscript “EP” in Eq. (12) denotes that this jet v_n^{jet} is defined via the event plane method. Shown in Fig. 4 are the angular distributions for $n = 2$ in $\Delta\phi_2$ for different centrality bins of Pb+Pb collisions at $\sqrt{s} = 2.76$ TeV, as compared to the corresponding ATLAS data [78]. Here, the jet radius is $R = 0.2$ and the jet transverse momentum is in the interval $60 < p_T < 80$ GeV/c.

We further fit these $\Delta\phi_2$ distributions with the function $2/(\pi\Delta p_T)(1 + 2v_2^{\text{jet,EP}} \cos(2\Delta\phi_2))$, as shown by the solid blue lines in Fig. 4, from which we extract the elliptic flow coefficient $v_2^{\text{jet,EP}}$. Here, the $2/\pi$ factor is introduced to normalize the jet spectrum within $\Delta\phi_2 \in [0, \pi/2]$. The corresponding values of $v_2^{\text{jet,EP}}$ are indicated in the figure for different centralities. We observe that for central collisions (5-10%), the jet elliptic coefficient is small due to the small geometric anisotropy of the average QGP profile. However, it is also non-zero due to the initial event-by-event geometrical fluctuation of the QGP. This $v_2^{\text{jet,EP}}$ increases with the centrality as the geometry of the QGP fireballs becomes more anisotropic towards semi-peripheral collisions. However, for very large centralities, $v_2^{\text{jet,EP}}$ decreases again, because the amount of jet energy loss is becoming smaller in these smaller systems, leading to a smaller $v_2^{\text{jet,EP}}$.

Similar results for Pb+Pb collisions at $\sqrt{s} = 5.02$ TeV are presented in Fig. 5. Both the azimuthal angular distributions of the jet yields (cross symbols) from LBT and their cosine function fits (solid lines) are shown for different centrality bins for jets with cone size $R = 0.2$ within $60 < p_T < 80$ GeV/c. The extracted $v_2^{\text{jet,EP}}$ from these cosine fits again first increases and then decreases with the centrality.

In Fig. 6, we summarize $v_2^{\text{jet,EP}}$ for jets with $100 < p_T < 200$ GeV/c from analyses of LBT results similar to what are presented in Figs. 4 and 5 in different centrality bins as a function of the average number of nucleon participants $\langle N_{\text{part}} \rangle$ in nuclear collisions at both $\sqrt{s} = 2.76$ and 5.02 GeV as compared to ATLAS data [78, 79]. As we have observed before, the jet elliptic anisotropy coefficient $v_2^{\text{jet,EP}}$ in these collisions first increases and then decreases with the participant number (as the centrality decreases), due to the competing effects between the geometric anisotropy and the initial size/temperature of the QGP medium. This centrality dependence from LBT

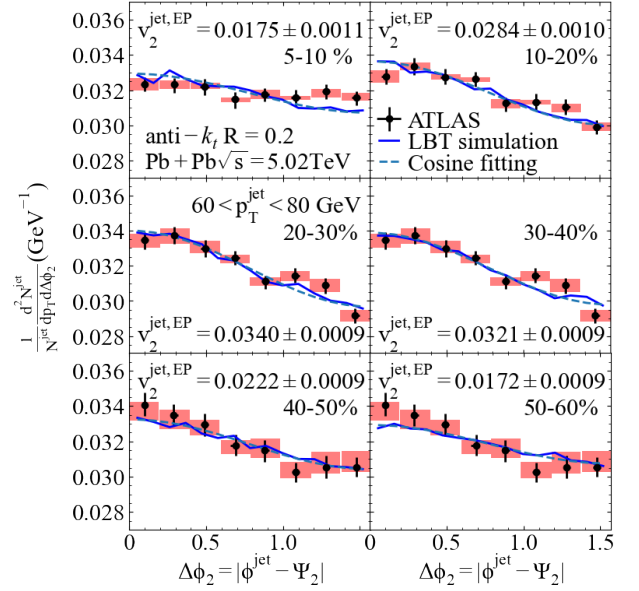


FIG. 5. (Color online) Distribution of the difference of the jet azimuthal angle ϕ^{jet} and the event plane angle Ψ_2 ($\Delta\phi_2 = \phi^{\text{jet}} - \Psi_2$) in different centrality bins of Pb+Pb collisions at $\sqrt{s} = 5.02$ TeV. Results calculated from the LBT model (blue solid lines) are compared to the ATLAS data [79] (black closed circle) and fitted with a cosine function (blue dash lines).

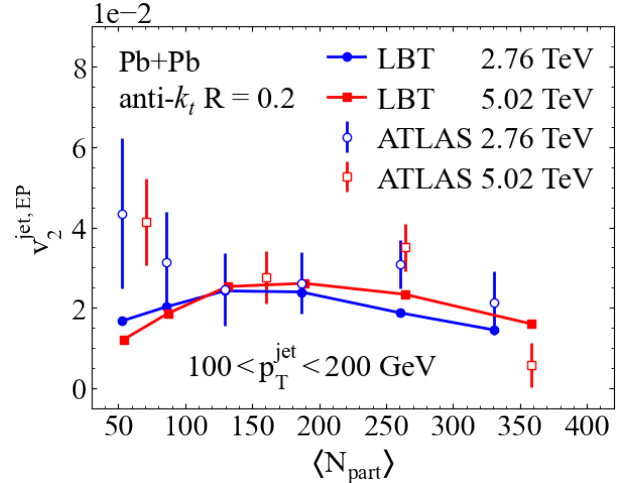


FIG. 6. (Color online) Jet elliptic anisotropy $v_2^{\text{jet,EP}}$ in $100 < p_T < 200$ GeV/c as a function of the number of participant nucleons N_{part} in Pb+Pb collisions at $\sqrt{s} = 2.76$ TeV (blue filled circle) and 5.02 TeV (red filled square) from LBT model calculations as compared to the ATLAS data [78, 79] (blue open circle and red open square).

simulations are consistent with the ATLAS data for central and semi-central Pb+Pb collisions at the LHC energies. The experimental data at more peripheral collisions are, however, somewhat higher than the LBT results. This might call into question on the validity of complete thermalization assumed in the hydrodynamic model

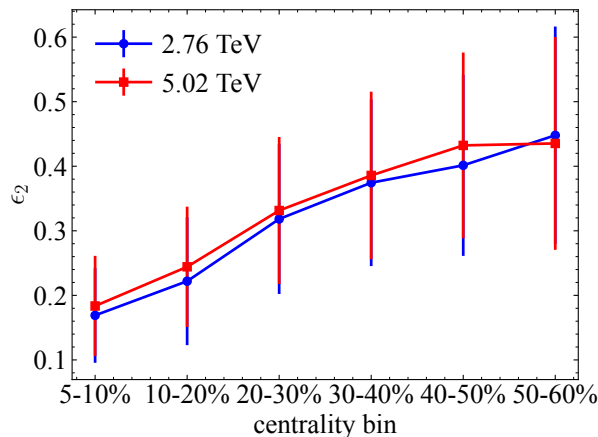


FIG. 7. (Color online) The initial second-order eccentricity ϵ_2 as a function of centrality in Pb+Pb collisions at $\sqrt{s} = 2.76$ TeV (blue circle) and 5.02 TeV (red square).

in small systems of peripheral collisions. The trigger bias and the neglect of impact-parameter dependence of nucleon-nucleon collisions in peripheral nuclear collisions [80] can potentially affect jet quenching and anisotropy analyses in these peripheral events. This can be clarified in the future by comparisons with experimental data from central light-ion, for example O+O, collisions [81] or p+A collisions [82].

Though there is no significant difference between experimental data on $v_2^{\text{jet,EP}}$ at the two colliding energies beyond systematic and statistic errors as shown in Fig. 6, there is a small but visible difference between LBT results at these two colliding energies. The small difference also depends on the centrality or the number of participant nucleons. For large values of $\langle N_{\text{part}} \rangle$ in central and semi-central collisions, $v_2^{\text{jet,EP}}$ at $\sqrt{s} = 5.02$ TeV is slightly larger than at 2.76 TeV. This variation can come from a combination of the colliding energy dependence of the jet energy loss (parton density at 5.02 TeV is higher than at 2.76 TeV), initial jet spectra (the spectra at 5.02 TeV is flatter than at 2.76 TeV) and the initial geometric anisotropy. This ordering is also similar to that of the elliptic flow coefficients for soft bulk hadrons in all centrality bins as summarized in Tab. I. However, unlike v_2^{soft} , the order for $v_2^{\text{jet,EP}}$ from LBT is reversed for small values of $\langle N_{\text{part}} \rangle$ in peripheral collisions as seen in Fig. 6. Since $v_2^{\text{jet,EP}}$ is directly driven by the initial geometric anisotropy of the QGP medium ϵ_2 instead of the final momentum anisotropy of soft hadrons v_2^{soft} , it is illustrative to exam the colliding energy dependence of the ϵ_2 coefficient from the AMPT model in Fig. 7. We indeed observe that the average values of ϵ_2 of the QGP medium in Pb+Pb collisions at $\sqrt{s} = 5.02$ TeV are larger than that at 2.76 TeV in central and semi-central collisions, except in the very peripheral collisions where the order is also reserved. A possible cause of the reversed ordering of $v_2^{\text{jet,EP}}$ and ϵ_2 in the colliding energy in peripheral col-

lisions is the amount of the geometric fluctuation of the corresponding bulk media. The fluctuation is expected to be larger at lower colliding energy, especially in peripheral collisions.

C. p_T dependence and effect of event fluctuation

Apart from extracting v_n^{jet} from the cosine function fit, we also use the following two methods to evaluate the jet anisotropy. The first one is equivalent to the cosine function fit, i.e., the event plane (“EP”) method, with the definition of the anisotropy as,

$$v_n^{\text{jet,EP}} = \langle \langle \cos(n[\phi^{\text{jet}} - \Psi_n]) \rangle \rangle, \quad (13)$$

where the symbol $\langle \langle \dots \rangle \rangle$ denotes the average over events. This event plane method does not take into account the fluctuation of the bulk v_n^{soft} within a given centrality bin. In the second approach, the scalar product (“SP”) method takes into account the correlation with v_n^{soft} fluctuation in the jet anisotropy,

$$v_n^{\text{jet,SP}} = \frac{\langle \langle v_n^{\text{soft}} \cos(n[\phi^{\text{jet}} - \Psi_n]) \rangle \rangle}{\sqrt{\langle v_n^{\text{soft}2} \rangle}}, \quad (14)$$

where v_n^{soft} represents the anisotropy of the soft bulk hadrons in one event, while $\sqrt{\langle v_n^{\text{soft}2} \rangle}$ denotes the root-mean-square average of v_n^{soft} within a given centrality bin.

In Fig. 8 we show the p_T dependence of v_2^{jet} with the above two different methods for Pb+Pb collisions with different centralities at both $\sqrt{s} = 2.76$ and 5.02 TeV, compared to the ATLAS data. The LBT results with the event plane (scalar product) method are shown as solid (dashed) lines that takes (does not take) into account of the fluctuation of soft hadron anisotropies v_n^{soft} . We find that the effect of the event-by-event fluctuation of the soft hadron v_2^{soft} on v_2^{jet} is negligibly small. We observe that v_2^{jet} in all centrality classes has a weak transverse momentum dependence, decreasing slightly with p_T . This is consistent with the p_T dependence of the single inclusive jet suppression factor $R_{\text{AA}}(p_T)$ which increases slightly with p_T as a result of the interplay between the p_T dependence of the jet energy loss and the shape of the initial jet spectra [60]. Again, the LBT model can describe the ATLAS data well except in very peripheral Pb+Pb collisions.

For a closer look at the effect of soft hadron v_2^{soft} fluctuation on jet v_2^{jet} , we present in Fig. 9 a comparison between the LBT results and the recent ATLAS data [79] on v_2^{jet} in Pb+Pb collisions at 5.02 TeV. Our LBT calculation provides a reasonable description of the experimental data. The inclusion of the soft hadron v_2^{soft} fluctuation increases the LBT results slightly on v_2^{jet} , though the effect is extremely small. This small relative difference is consistent with the estimate $(\delta v_2^{\text{soft}}/v_2^{\text{soft}})^2 \sim 0.01 - 0.02$ according to Tab. I. It is also consistent with the findings

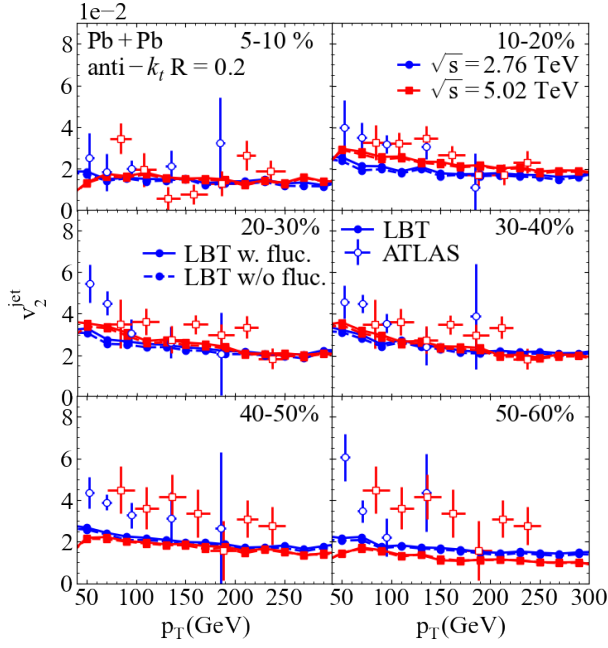


FIG. 8. (Color online) Jet elliptic anisotropy coefficient v_2^{jet} as a function of the jet p_T from the LBT model (closed marker) as compared to the ATLAS data [78, 79] (open marker) in different centrality ranges of Pb+Pb collisions at $\sqrt{s} = 2.76$ TeV (blue circle) and 5.02 TeV (red square). $v_2^{\text{jet,SP}}$ is labeled as “with (soft v_2) fluctuations” (solid lines), and $v_2^{\text{jet,EP}}$ is labeled as “without fluctuations” (dashed lines).

for the elliptic flow of single inclusive hadrons in an earlier study [83]. This is, however, in sharp contrast to the conclusion in Ref.[36] where the effect of bulk flow fluctuation was found significantly larger for high p_T single inclusive hadrons.

Again, the experimental data in Fig. 8 show no significant dependence on the colliding energy. The LBT results have the same small colliding energy dependence, consistent with the findings in Fig. 6. The jet elliptic anisotropy v_2^{jet} is slightly larger or smaller in collisions at $\sqrt{s} = 2.76$ TeV than at 5.02 TeV depending on the centrality, due to the centrality dependence of the different bulk geometric anisotropy ϵ_2 produced at these two colliding energies as we have just discussed in the above subsection.

D. Soft and hard correlation

The geometric anisotropy of the QGP medium is expected to be the dominant factor that determines the jet anisotropy v_n^{jet} due to the length dependence of transverse momentum broadening and parton energy loss. This geometric anisotropy fluctuates from event to event even for a given centrality class as reflected by the fluctuation of the anisotropic flow coefficients of soft bulk hadrons shown in Figs. 2 and 3. Since the anisotropic

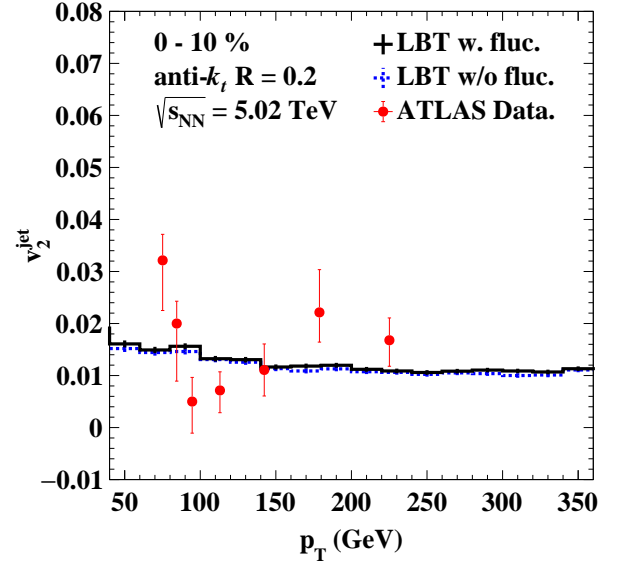


FIG. 9. (Color online) Jet elliptic anisotropy coefficient v_2^{jet} as a function of the jet p_T from the LBT model calculation (lines) as compared to the ATLAS data [79] (markers) in 0-10% Pb+Pb collisions at $\sqrt{s} = 5.02$ TeV. $v_2^{\text{jet,SP}}$ is labeled as “with (soft v_2) fluctuations” (solid lines), and $v_2^{\text{jet,EP}}$ is labeled as “without fluctuations” (dashed lines).

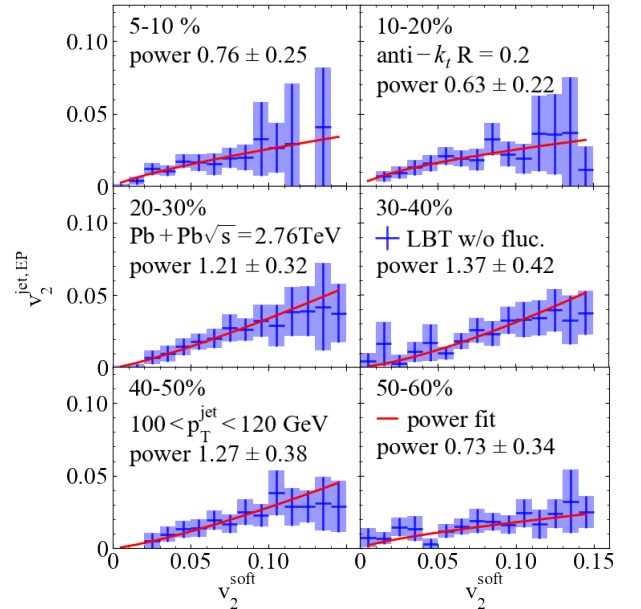


FIG. 10. (Color online) Correlations between $v_2^{\text{jet,EP}}$ and the bulk v_2^{soft} in Pb+Pb collisions at $\sqrt{s} = 2.76$ TeV with jet transverse momentum $100 < p_T < 120$ GeV/c. The LBT results (blue points with error boxes) is fitted with a power law correlation (red lines) in each centrality bin with the power index as indicated.

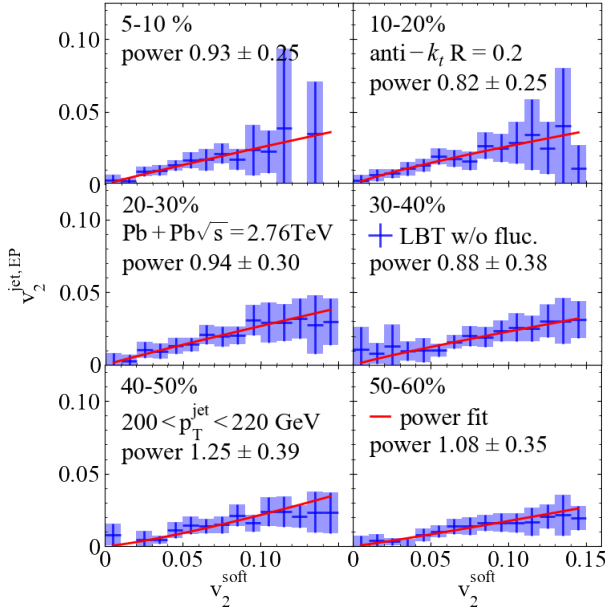


FIG. 11. (Color online) Correlations between $v_2^{\text{jet,EP}}$ and the bulk v_2^{soft} in Pb+Pb collisions at $\sqrt{s} = 2.76$ TeV with jet transverse momentum $200 < p_T < 220$ GeV/c. The LBT results (blue points with error boxes) is fitted with a power law correlation (red lines) in each centrality bin with the power index as indicated.

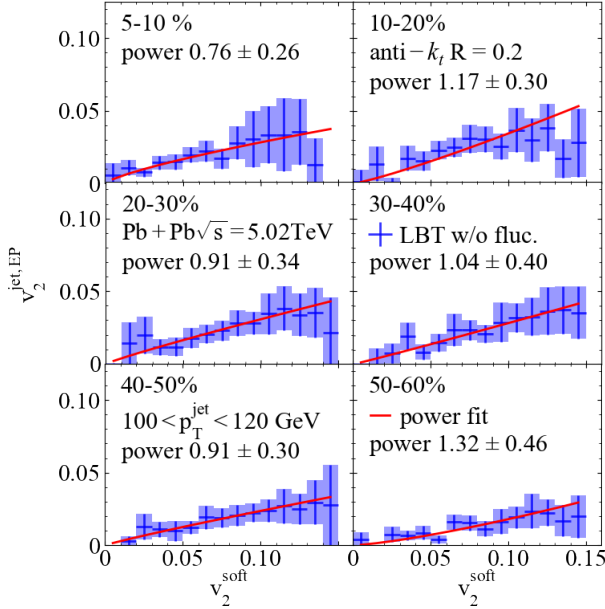


FIG. 12. (Color online) Correlations between $v_2^{\text{jet,EP}}$ and the bulk v_2^{soft} in Pb+Pb collisions at $\sqrt{s} = 5.02$ TeV with jet transverse momentum $100 < p_T < 120$ GeV/c. The LBT results (blue points with error boxes) is fitted with a power law correlation (red lines) in each centrality bin with the power index as indicated.

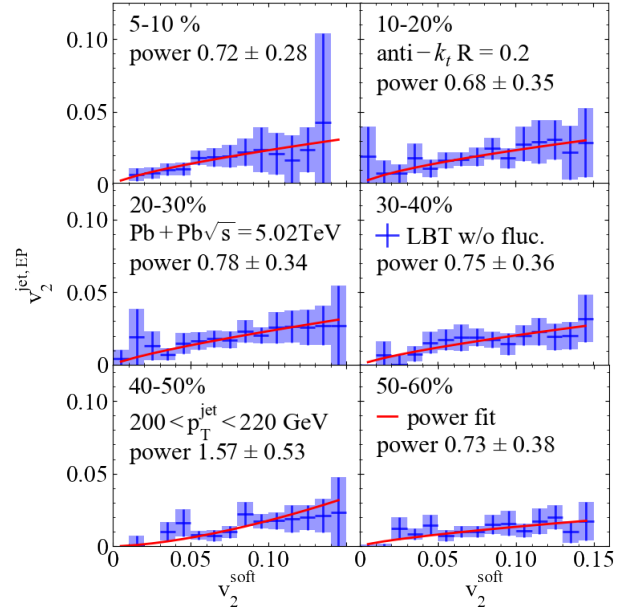


FIG. 13. (Color online) Correlations between $v_2^{\text{jet,EP}}$ and the bulk v_2^{soft} for different centralities of $\sqrt{s} = 5.02$ TeV Pb+Pb collisions with jet transverse momentum within $200 < p_T < 220$ GeV. The LBT results (blue points with error boxes) is fitted with a power law (red lines).

flows of soft hadrons are also driven by the initial geometric anisotropies of the QGP medium, one should expect a direct event-by-event correlation between the anisotropic flow of soft hadrons v_2^{soft} and the jet anisotropy v_2^{jet} .

In Figs. 10, 11, 12 and 13, we show the correlation between the soft hadron v_2^{soft} and the jet elliptic anisotropy v_2^{jet} in different jet p_T ranges for different centrality classes of Pb+Pb collisions at the LHC energies as simulated by LBT and CLVisc. Results for both $\sqrt{s} = 2.76$ TeV (Figs. 10 and 11) and 5.02 TeV (Figs. 12 and 13) are presented. In each panel of these figures, blue crosses represent results from our LBT and CLVisc calculations, while red curves represent a power law fit in the following form,

$$v_2^{\text{jet}} = \alpha (v_2^{\text{soft}})^\beta, \quad (15)$$

with α as an overall normalization factor and β as the power index. Both anisotropies are analyzed with event plane method. Note that for any given value of v_2^{soft} in each hydro event, the jet anisotropy v_2^{jet} from the event plane method in Eq. (13) and the scalar product method in Eq. (14) coincide. One observes that the power indices β from the fitting are all around 1, indicating an approximately linear correlation between the jet $v_2^{\text{jet,EP}}$ and the bulk v_2^{soft} due to the fluctuation of the bulk medium. This linear correlation is quite interesting and not necessarily straightforward since the bulk hadron anisotropy arises from collective expansion while the jet anisotropy is caused by the length dependence of parton energy loss. The initial geometrical anisotropy of the expanding QGP

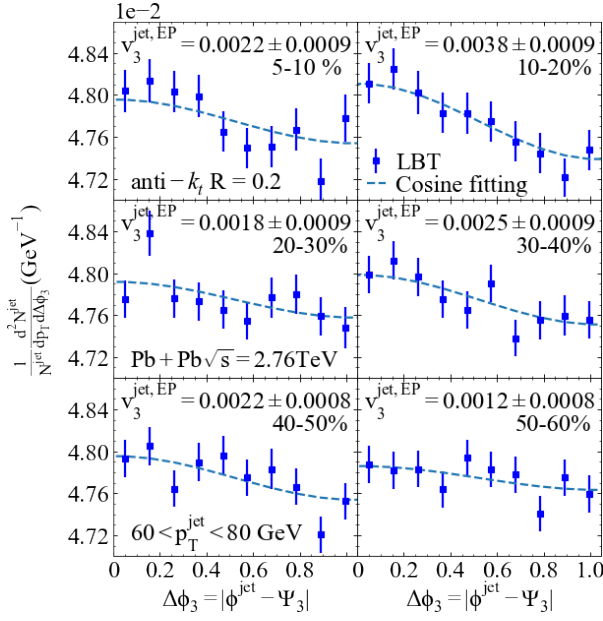


FIG. 14. (Color online) Distributions of the difference of the jet azimuthal angle ϕ^{jet} and the event plane angle Ψ_3 ($\Delta\phi_3 = \phi^{\text{jet}} - \Psi_3$) for different centrality bins of Pb+Pb collisions at $\sqrt{s} = 2.76$ TeV. Results calculated from the LBT model (blue solid squares) are fitted with a cosine function (blue dash lines).

fireball is the link underlying this correlation. We have tried to include only elastic processes in the LBT simulations with increased effective coupling constant so that one can still fit the experimental data on single inclusive jet suppression $R_{\text{AA}}^{\text{jet}}$. This model simulation leads to only a slightly different length dependence of jet energy loss. However the resultant soft and hard correlation between v_2^{jet} and v_2^{soft} still remains approximately linear. One probably needs to have a joint analysis of the centrality dependence of the single inclusive jet suppression $R_{\text{AA}}^{\text{jet}}$ and jet anisotropy v_2^{jet} and the soft hard correlation between v_2^{jet} and v_2^{soft} in order to provide a stringent constraint on the jet transport dynamics. This is however beyond the scope of the study in this paper.

V. SINGLE INCLUSIVE JET ANISOTROPY v_3^{jet}

In addition to the elliptic flow coefficient, we can also study the triangular flow coefficient v_3^{jet} of jets, which helps place more stringent constraints on the jet transport dynamics inside the QGP medium as well as the effect of bulk medium fluctuation on jet observables.

Similar to the discussion about the elliptic jet anisotropy in the previous section, we first present the azimuthal angle distribution of single inclusive jets within $60 < p_T < 80$ GeV in Pb+Pb collisions at $\sqrt{s} = 2.76$ TeV in Fig. 14, and at 5.02 TeV in Fig. 15. The horizontal axis $\Delta\phi_3 \equiv \phi^{\text{jet}} - \Psi_3$ is defined as the differ-

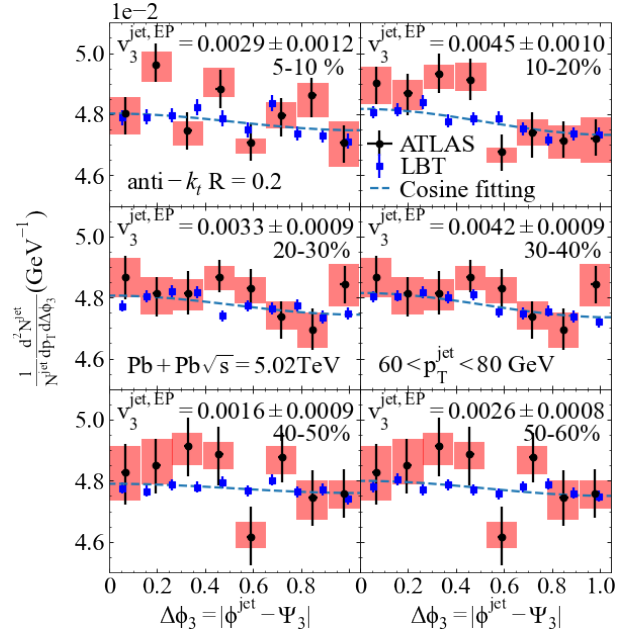


FIG. 15. (Color online) Distributions of the difference of the jet azimuthal angle ϕ^{jet} and the event plane angle Ψ_3 ($\Delta\phi_3 = \phi^{\text{jet}} - \Psi_3$) for different centrality bins of Pb+Pb collisions at $\sqrt{s} = 5.02$ TeV. Results calculated from the LBT model (blue solid squares) are compared with the ATLAS data [79] (black closed circle) and fitted with a cosine function (blue dash lines).

ence between the azimuthal angle of the jet ϕ^{jet} and the 3rd-order event plane angle Ψ_3 of the bulk hadrons. We then fit the jet distribution in $\Delta\phi_3$ from the LBT calculations (solid blue squares) with a cosine function $3/(\pi\Delta p_T)(1 + 2v_3^{\text{jet,EP}} \cos(3\Delta\phi_3))$ (dashed lines), where the $3/\pi$ factor is introduced to normalize the distribution function within $[0, \pi/3]$. Since such a fitting corresponds to the event plane method, we label the jet triangular anisotropy coefficient as $v_3^{\text{jet,EP}}$. The extracted values of $v_3^{\text{jet,EP}}$ are presented in different panels for various classes of centrality.

To summarize the centrality dependence of v_3^{jet} and compare the results at two colliding energies, we present $v_3^{\text{jet,EP}}$ as a function of the number of participant nucleons in Fig. 16 for jets with the cone size $R = 0.2$ and transverse momentum $100 < p_T < 200$ GeV/c in different centrality classes of Pb+Pb collisions at $\sqrt{s} = 2.76$ and 5.02 TeV. One observes that $v_3^{\text{jet,EP}}$ in general is larger in central collisions (large N_{part}) than in peripheral collisions (small N_{part}). This is different from the centrality dependence of the elliptic jet anisotropy coefficient v_2^{jet} as previously shown in Fig. 6. The triangular geometric anisotropy ϵ_3 of the bulk medium results from the initial state fluctuation while the elliptic geometric anisotropy ϵ_2 is mainly caused by the shape of the nuclear overlap in non-central collisions, though ϵ_2 in the most central collisions also comes from initial fluctuations. As illus-

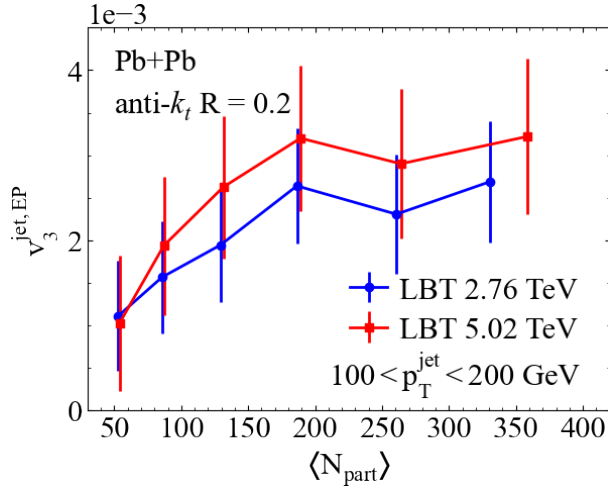


FIG. 16. (Color online) The jet $v_3^{\text{jet,EP}}$ within $100 < p_T < 200$ GeV/c as a function of the number of participant nucleons N_{part} in Pb+Pb collisions at $\sqrt{s} = 2.76$ TeV (blue circles with line) and 5.02 TeV (red squares with line).

trated in Tab. II, the bulk v_3^{soft} has a very weak centrality dependence. This should be the same for the triangular geometric anisotropy of the bulk medium. Therefore, larger energy loss of jets in more central collisions naturally gives rise to larger $v_3^{\text{jet,EP}}$ than that in peripheral collisions. On the other hand, the elliptic geometric anisotropy of the nuclear overlap is strongly correlated with the centrality, decreasing toward central collisions. This decrease can overcome the increased jet energy loss such that the final jet elliptic anisotropy $v_2^{\text{jet,EP}}$ also decreases toward central collisions as seen in Fig. 6.

Compared to Fig. 6 for the centrality dependence of the jet elliptic anisotropy, we observe that the values of the jet triangular anisotropy v_3^{jet} from LBT in Fig. 16 are almost an order of magnitude smaller than those of the jet elliptic anisotropy v_2^{jet} . However, these are still significantly larger than the triangular anisotropy of large transverse momentum single inclusive hadron spectra predicted in Ref. [36]. We also observe that the jet triangular anisotropy $v_3^{\text{jet,EP}}$ in Pb+Pb collisions at $\sqrt{s} = 5.02$ TeV from LBT simulations is larger than that at 2.76 TeV for all the centrality classes. Since the geometrical triangular anisotropies of the systems are similar between the two colliding energies as indicated by the bulk triangular flow coefficients shown in Tab. II, this change of jet triangular anisotropy with the colliding energy from 2.76 to 5.02 TeV is mainly caused by the increase of jet energy loss as the initial parton density and the jet transport coefficient increase by about 20%, indicated by the similar increase in the charged hadron multiplicity in the central rapidity region [84, 85].

Shown in Fig. 17 is the transverse momentum dependent v_3^{jet} in Pb+Pb collisions at both $\sqrt{s} = 2.76$ and 5.02 TeV, as compared to the ATLAS data. Though the ATLAS data are consistent with LBT results, the ex-

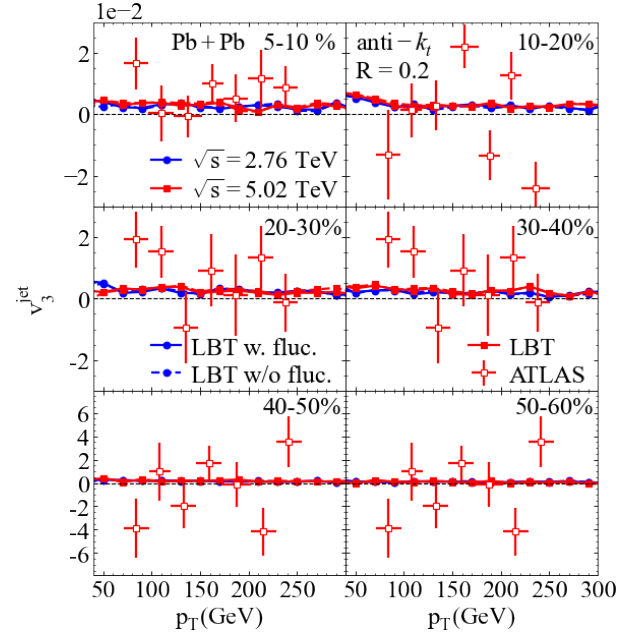


FIG. 17. (Color online) The jet v_3^{jet} as a function of the jet p_T in different centralities of Pb+Pb collisions at $\sqrt{s} = 2.76$ TeV (blue circles) and 5.02 TeV (red squares) from the LBT model calculation (closed marker) as compared to the ATLAS data [79] (open marker), $v_3^{\text{jet,SP}}$ is labeled as “with (soft v_3) fluctuations” (solid lines) while $v_3^{\text{jet,EP}}$ is labeled as “without fluctuations” (dashed lines).

perimental errors, mainly statistical, have to be significantly reduced in order to observe the small jet triangular anisotropy.

To exam the colliding energy and transverse momentum dependence and the effect of bulk flow fluctuations in more detail, we present the same LBT results in Fig. 18 with an increased resolution of the vertical axis. We observe the same colliding energy dependence as discussed above. It also decreases slightly with the jet transverse momentum, similar to the p_T dependence of v_2^{jet} . By comparing the results with bulk flow fluctuations (solid lines) using the scalar product method in Eq. (14) and that without flow fluctuations (dashed lines) using the event plane method Eq. (13), it is, however, difficult to see the effect of the bulk flow fluctuations because of the limited statistics of the LBT simulations in these centrality classes.

To better illustrate the effect of the bulk flow fluctuations, we present v_3^{jet} from LBT simulations with much higher statistics in Fig. 19 as a function of the jet p_T in 0-10% Pb-Pb collisions at $\sqrt{s} = 5.02$ TeV. Similar to the conclusion drawn for v_2^{jet} , the event plane method and the scalar product method lead to very similar values of the jet v_3^{jet} , indicating negligible effect of the event-by-event bulk flow fluctuations. The results from LBT calculations are consistent with the more recent ATLAS data [79] with smaller statistic errors. The small v_3^{jet} from LBT is clearly seen to decrease with jet p_T , similar

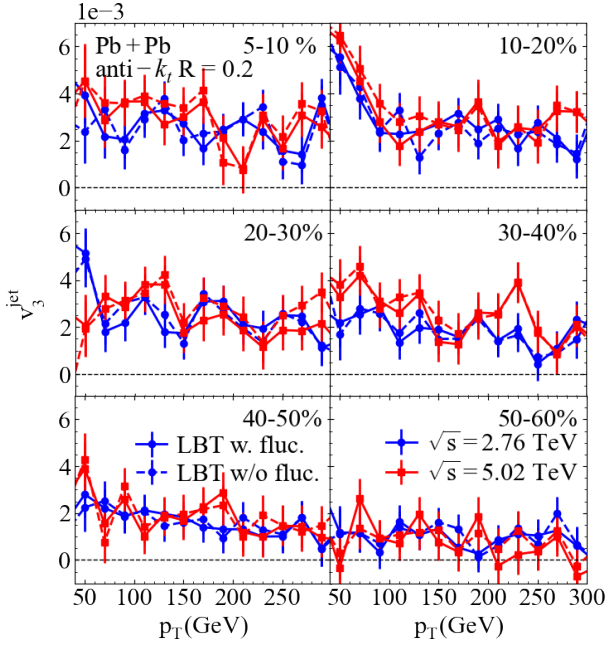


FIG. 18. (Color online) The jet v_3^{jet} as a function of the jet p_T in different centralities of Pb+Pb collisions at $\sqrt{s} = 2.76$ TeV (blue circles) and 5.02 TeV (red squares) from the LBT calculations using the event plane analysis $v_3^{\text{jet,EP}}$ (labeled as “with soft v_3 fluctuations” – solid lines) and scalar product analysis $v_3^{\text{jet,SP}}$ (labeled as “without fluctuations” – dashed lines).

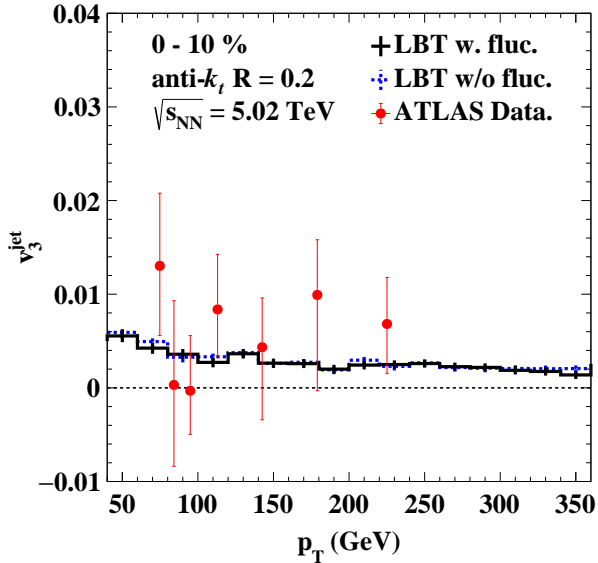


FIG. 19. (Color online) The jet v_3^{jet} as a function of the jet p_T in 0-10% Pb+Pb collisions at $\sqrt{s} = 5.02$ TeV from the LBT model analyzed with the event plane method (without fluctuation) (dashed line) and scalar product method (with fluctuation) (solid line) as compared to the ATLAS data [79].

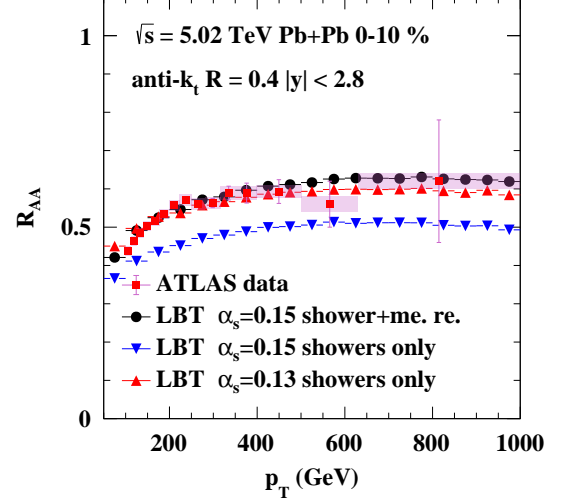


FIG. 20. (Color online) Suppression factors of single inclusive jets ($R = 0.4$) R_{AA} in 0-10% Pb+Pb collisions at $\sqrt{s} = 5.02$ TeV from LBT with (black circle) and without (blue triangle down) jet-induced medium response for $\alpha_s = 0.15$ or without jet-induced medium response but for $\alpha_s = 0.13$ (red triangle up), as compared to the ATLAS data [86].

to v_2^{jet} shown in Fig. 9.

VI. EFFECT OF MEDIUM RESPONSE ON v_2^{jet}

One important motivation for developing the LBT model is to investigate the propagation of recoil medium partons and the back-reaction partons on the same footing as the jet shower partons (both leading jet shower partons and radiated gluons induced by jet-medium interaction). Since some of the final hadrons from the hadronization of the recoil medium partons can still fall inside the jet-cone, they will contribute to the total jet energy within the jet cone. The back-reaction induced by the parton transport essentially depletes the phase-space of medium partons behind the propagating jet which is often referred to as the diffusion wake. The energy of these back-reaction medium, or “negative partons” within the jet-cone has to be subtracted from the total jet energy. We generally refer recoil and back-reaction or “negative” partons as jet-induced medium response.

Effects of jet-induced medium response on net jet energy loss and jet suppression within the LBT and the CoLBT-hydro model have been discussed in detail in previous studies on single inclusive jets [60], γ/Z_0 -jets [61, 62], as well as γ/Z_0 -hadron correlations [66, 68] and γ -jet fragmentation functions [67] in heavy-ion collisions. Effects of jet-induced medium response have also been studied within other models such as the MARTINI [87, 88], JEWEL [89, 90], Hybrid [91, 92] and the coupled

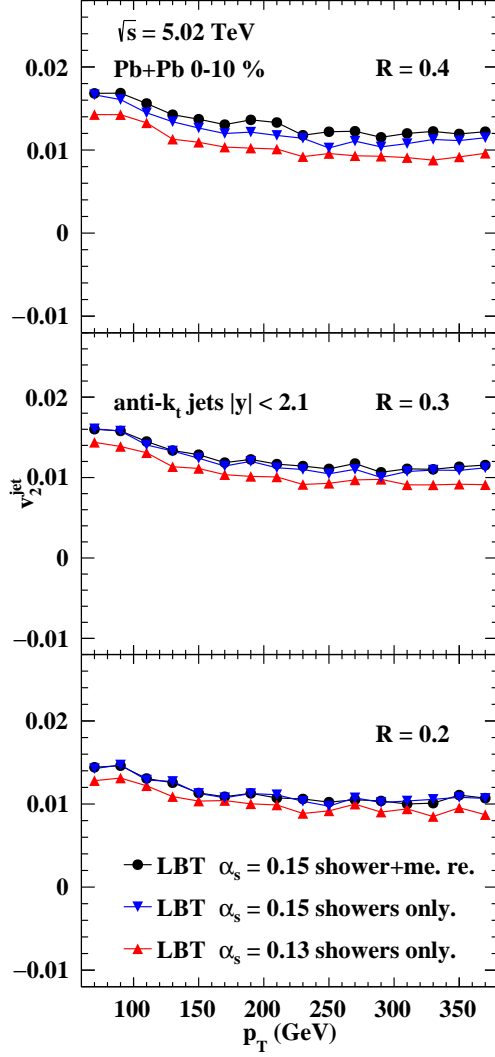


FIG. 21. (Color online) Inclusive jet azimuthal anisotropy v_2^{jet} in 0-10% Pb+Pb collisions at $\sqrt{s} = 5.02$ TeV with jet cone size $R = 0.2, 0.3, 0.4$ in mid-rapidity range calculated within the LBT model with (black circle) and without (blue triangle down) jet-induced medium response for $\alpha_s = 0.15$ or without jet-induced medium response but for $\alpha_s = 0.13$ (red triangle up).

jet-fluid model [93]. For a recent review on jet quenching and jet-induced medium response see Ref. [7]. The jet-induced medium response is found to reduce the net jet energy loss and therefore the jet suppression while it enhances soft hadron production both toward the outer edge and outside of the jet cone. It is expected that its effects will also depend on the azimuthal angle of the jet propagation relative to the event plane of the bulk medium. It should therefore also influence the jet azimuthal anisotropy.

Since the inclusion of jet-induced medium response in the jet reconstruction reduces the net jet energy loss,

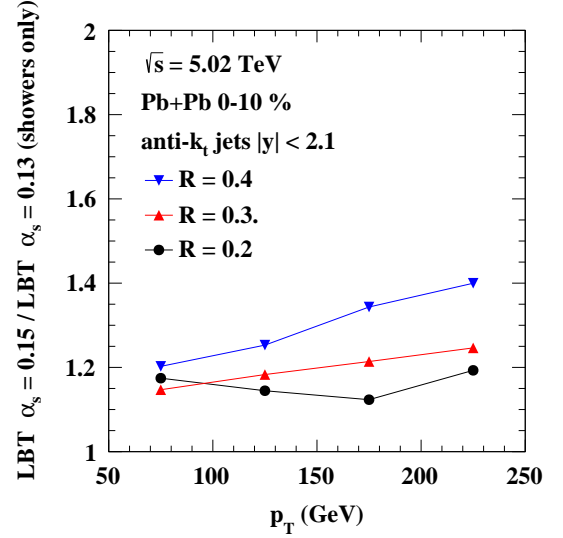


FIG. 22. (Color online) The ratio of inclusive v_2^{jet} between with medium response effect (at $\alpha_s = 0.15$) and without medium response effect (at $\alpha_s = 0.13$) in the 0-10% centrality and mid-rapidity range of 5.02 TeV Pb+Pb collisions with jet cone size $R = 0.2$ (black circle), 0.3 (blue triangle down) and 0.4 (red triangle up).

it is also expected to reduce the jet suppression as well as the jet azimuthal anisotropies. Jet energy loss and suppression are generally positively correlated with jet anisotropies. To examine the effect of jet-induced medium response on jet anisotropies beyond such a trivial correlation with the net jet energy loss, we adjust the effective strong coupling constant α_s so that the net jet energy loss and the jet suppression remain the same as in the case when jet-induced medium response is included. Shown in Fig. 20 are the jet suppression factors R_{AA} for jet cone size $R = 0.4$ from LBT simulations of 0-10% central Pb+Pb collisions at $\sqrt{s} = 5.02$ TeV with (black circle) and without (blue triangle down) medium response for $\alpha_s = 0.15$ as compared to the ATLAS experimental data [86]. Without the medium response, LBT results at this effective strong coupling constant have too much suppression as compared to the experimental data. In order to fit the experimental data without the jet-induced medium response, one can reduce the effective strong coupling constant to $\alpha_s = 0.13$ (red triangle up). We show in Fig. 21 the corresponding v_2^{jet} with (black circle) and without (blue triangle down) medium response with the same effective coupling constant and a reduced effective coupling constant (red triangle up) tuned to fit the jet suppression factor. We can see there are noticeable differences in the jet azimuthal anisotropy when jet-induced medium response is excluded from jet reconstruction even when the effective coupling constant is tuned to fit the overall jet suppression. The difference increases with the jet cone-size.

To exam the azimuthal dependence of the effect of the

jet-induced medium response beyond the simple path length dependence of net jet energy loss, we plot the ratios of the jet elliptic anisotropy from LBT with and without jet-induced anisotropy (but with reduced effective coupling constant so that the jet suppression remains the same) in Fig. 22 for different jet cone sizes. One can see that the medium response increases v_2^{jet} by about 20~40% in the p_T range of 50~250 GeV/c as compared to the case without medium response even when LBT is tuned in both cases to give the same averaged jet suppression. The increase is bigger for a larger jet cone-size.

While the azimuthal dependence of the averaged jet path length is the dominant mechanism for the azimuthal anisotropy of jet suppression, it has the opposite effect on the influence of medium response on jet anisotropy. Long (short) path length causes more (less) jet-induced medium response which leads to more (less) reduction of the net jet energy loss and less (more) jet suppression. Therefore such length dependence of the medium response reduces jet anisotropy. However, the combined effect of radial flow and jet-induced medium response can increase jet anisotropy. According to the study of jet energy loss in Ref. [60], radial flow tends to increase the effect of jet-induced medium response and further reduces the net jet energy loss and leads to less jet suppression. This effect of radial flow is bigger for a larger jet cone size. Consequently, the azimuthal modulation of the radial flow, which gives rise to the bulk anisotropic flow, will increase the jet anisotropy. The increase should be bigger for jets with a larger cone size since they contain more contribution from jet-induced medium excitation. These are exactly what we observe in the LBT calculations as shown in Fig. 22. The LBT results clearly demonstrate that when jet R_{AA} is fixed, incorporating the medium response increases v_2^{jet} , and stronger enhancement is obtained for jets with larger cone sizes. This also implies that the effect of jet-induced medium response on the reconstructed jet energy is influenced by the radial flow which changes with the azimuthal angle relative to the event plane. The effect understandably increases with the jet cone-size.

VII. EFFECT OF VISCOSITY ON v_2^{jet}

So far the hydrodynamic profiles of the bulk medium we have used in the LBT model to calculate the jet anisotropy were given by the CLVisc simulations for an ideal quark-gluon plasma with zero shear viscosity $\eta = 0$. However, the shear viscosity of QGP is known to be critical for a more realistic description of the anisotropic flows of the bulk medium with given initial conditions. It is therefore also important to check the effect of the viscosity of the bulk medium on jet quenching, jet anisotropy and hard-soft correlation.

We carry out the same simulations and jet analyses within LBT in which the space-time profiles of the bulk medium are given by CLVisc hydrodynamic model with

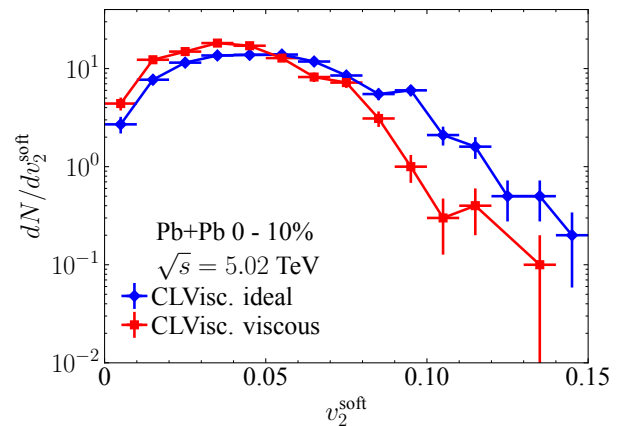


FIG. 23. (Color online) Distributions of soft hadron v_2^{soft} ($0.3 < p_T < 3$ GeV/c) from CLVisc model simulations of 0-10% central Pb+Pb collisions at $\sqrt{s} = 5.02$ TeV with shear viscosity to entropy density ratio $\eta/s = 0.08$ (red square) and $\eta/s = 0$ (blue diamonds). Errors are statistical with 1000 hydro events.

the same initial conditions but with finite shear viscosity $\eta/s = 0.08$. The overall scale factor K in the initial conditions for the hydrodynamics in Eq. (11) is adjusted so that the final charged hadron rapidity density in the most central collisions remains the same in ideal and viscous hydrodynamic calculations as compared to the experimental data. Shown in Fig. 23 are the distributions of soft hadron elliptic anisotropy v_2^{soft} in 0-10% central Pb+Pb collisions at $\sqrt{s} = 5.02$ TeV calculated with CLVisc with shear viscosity to entropy density ratio $\eta/s = 0$ (blue diamonds) and $\eta/s = 0.08$ (red square). Within the statistic errors for 1000 hydro events, the v_2^{soft} distributions from ideal and viscous CLVisc hydrodynamic evolution are similar, except that both the average value and the tail of fluctuation from the viscous hydro are smaller than that from the ideal hydro as expected. Note that we have imposed a cut in $0.3 < p_T < 3$ GeV/c in this calculation of v_2^{soft} as in the experimental analysis [74, 75] which also influences the v_2^{soft} distribution slightly.

Using the space-time parton density profiles from these viscous and ideal hydrodynamic events, we first compare in Fig. 24 the suppression factors of single inclusive jets (with cone size $R = 0.4$) R_{AA} in 0-10% Pb+Pb collisions at $\sqrt{s} = 5.02$ TeV from LBT with viscous (green solid line) and ideal (blue dashed line) hydro profiles with the same effective coupling constant $\alpha_s = 0.15$, as compared to the ATLAS data [86]. Since the entropy density is slightly larger in the viscous hydro than that in the ideal hydro, the corresponding jet energy loss is also larger and jets are slightly more suppressed in the viscous hydro than in the ideal hydro. However, the difference is very small.

Similarly, we show the jet elliptic flow coefficient v_2^{jet} as a function of the jet p_T from LBT model calculations with viscous (blue square-line) and ideal (green diamond-line)

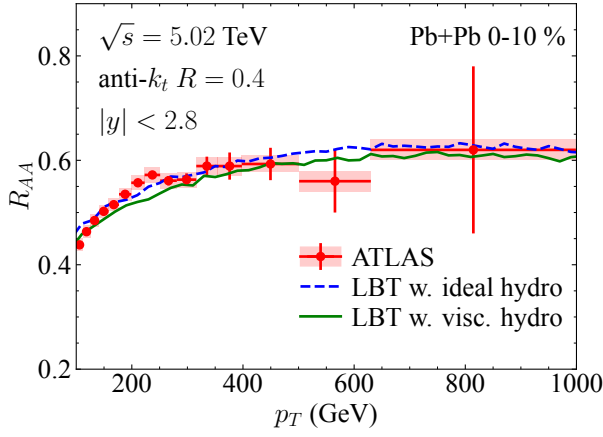


FIG. 24. (Color online) Suppression factors of single inclusive jets ($R = 0.4$) R_{AA} in 0-10% Pb+Pb collisions at $\sqrt{s} = 5.02$ TeV from LBT with (green solid line) and without (blue dash line) viscosity at $\alpha_s = 0.15$, as compared to the ATLAS data [86].

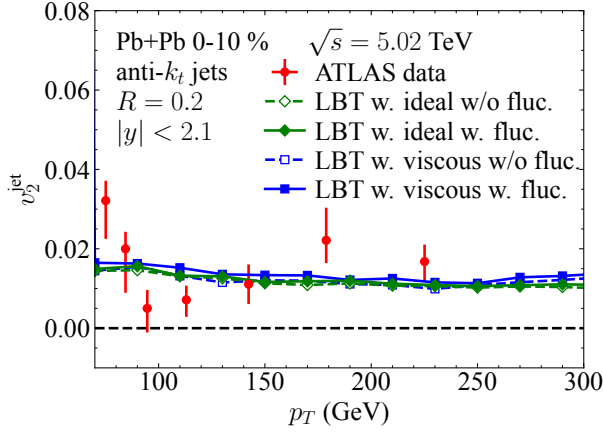


FIG. 25. (Color online) The jet elliptic flow coefficient v_2^{jet} as a function of the jet p_T from the LBT model calculations with ideal (green diamond) and viscous (blue square) hydro profiles as compared to the ATLAS data [79] (filled red circles) in 0-10% Pb+Pb collisions at $\sqrt{s} = 5.02$ TeV. $v_2^{\text{jet,SP}}$ is labeled as “with (soft v_2) fluctuations” (filled symbol and solid line), and $v_2^{\text{jet,EP}}$ is labeled as “without fluctuations” (open symbol and dashed line).

hydro profiles as compared to the ATLAS data [79] (filled red circles) in 0-10% Pb+Pb collisions at $\sqrt{s} = 5.02$ TeV in Fig. 25. $v_2^{\text{jet,SP}}$ is labeled as “with (soft v_2) fluctuations” (filled-symbol and solid lines), and $v_2^{\text{jet,EP}}$ is labeled as “without fluctuations” (open-symbol and dashed lines). One finds that the viscous hydro enhances jet anisotropy slightly, which is mainly due to the larger jet quenching in the viscous hydro than in the ideal hydro, consistent with the effect of viscosity on jet suppression factor R_{AA} in Fig. 24.

Finally, we show in Fig. 26 the correlation between $v_2^{\text{jet,EP}}$ and the bulk v_2^{soft} ($0.3 < p_T < 3$ GeV/c) in 0-

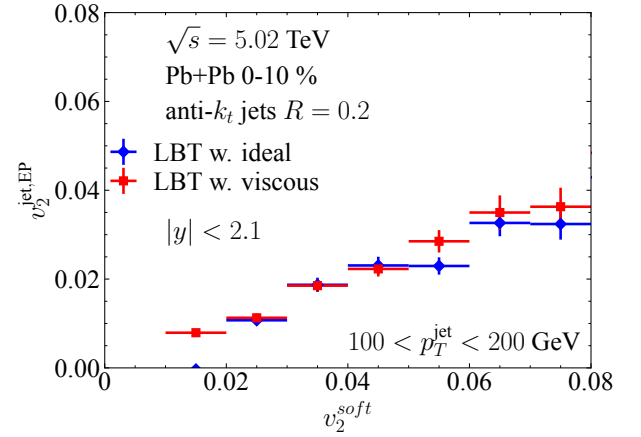


FIG. 26. (Color online) Correlations between $v_2^{\text{jet,EP}}$ and bulk v_2^{soft} in 0-10% Pb+Pb collisions $\sqrt{s} = 5.02$ TeV with jet transverse momentum $100 < p_T < 200$ GeV/c from LBT simulations with viscous (red square) and ideal (blue diamond) hydro profiles.

10% Pb+Pb collisions at $\sqrt{s} = 5.02$ TeV with jet transverse momentum $100 < p_T < 200$ GeV/c with viscous (red squares) and ideal (blue diamonds) hydro profiles in LBT. The correlation between jet and soft bulk elliptic flow coefficients in viscous and ideal hydro are almost identical in the region $0.1 < v_2^{\text{soft}} < 0.4$ since the distributions of v_2^{soft} in both cases are very similar. In the large region of $v_2^{\text{soft}} > 0.4$, the fluctuation of the bulk v_2^{soft} in the viscous hydro is smaller than that in the ideal hydro (see Fig. 23). This results in a slightly larger correlation between $v_2^{\text{jet,EP}}$ and v_2^{soft} in the viscous hydro than that in an ideal hydro.

VIII. SUMMARY

We have studied in this paper the azimuthal anisotropic coefficients of single inclusive jets produced in relativistic heavy-ion collisions within the LBT model. The AMPT model is used to consistently generate the initial geometric distribution of both the energy density profile for the hydrodynamic evolution of the bulk medium and jet production vertices for jet transport within LBT. The subsequent evolution of the QGP medium is simulated using the CLVisc hydrodynamic model, while the jet-medium interactions are simulated using the LBT model. The only additional model parameter in LBT, the effective strong coupling constant $\alpha_s = 0.15$, was fixed in our earlier work [60] that provided satisfactory description of the single inclusive jet suppression R_{AA} in Pb+Pb collisions at both $\sqrt{s} = 2.76$ and 5.02 TeV. Different analysis methods for extracting the anisotropic coefficients of jets have been applied and compared, including the cosine function fit from the azimuthal angular distribution of jets, the event plane method and the scalar product method. Within this framework, we have investigated

the transverse momentum dependence, the centrality or participant nucleon number dependence, as well as the colliding energy dependence of the jet anisotropies v_n^{jet} . Effects of jet-induced medium excitation and viscosity of the bulk medium on the jet v_2^{jet} have also been discussed in detail.

We found that, as the centrality increases or the number of participant nucleons decreases, the v_2^{jet} coefficient for jets produced in Pb+Pb collisions at both $\sqrt{s} = 2.76$ and 5.02 TeV first increases and then decreases. This non-monotonic behavior, similar to the centrality dependence of v_2^{soft} for soft hadrons, results from the competition between the elliptic geometric anisotropy (ϵ_2) of the QGP medium and the amount of net jet energy loss – the former is larger in more peripheral collisions while the latter is larger in more central collisions. In contrast, the v_3^{jet} coefficient appears monotonically decreasing as the centrality increases, for jets produced at both $\sqrt{s} = 2.76$ and 5.02 TeV, since the triangular geometric anisotropy (ϵ_3) of the QGP fireball only weakly depends on centrality and v_3^{jet} is mainly driven by jet energy loss which decreases monotonically with centrality. Comparing results at the two colliding energies, we noticed that v_2^{jet} is larger at $\sqrt{s} = 5.02$ TeV than at 2.76 TeV when N_{part} is large, but smaller when N_{part} is small. This can be understood with the larger ϵ_2 of the QGP profile at $\sqrt{s} = 5.02$ TeV than at 2.76 TeV in central collisions, but possible smaller ϵ_2 in peripheral collisions within the AMPT model. In contrast, v_3^{jet} remains larger at 5.02 TeV than at 2.76 TeV across the kinematic and centrality region explored in this work. Our study has shown little difference of the v_2^{jet} and v_3^{jet} coefficients between analyses using the event plane method and the scalar product method, indicating very weak dependence of v_n^{jet} on the event-by-event fluctuation of the bulk v_n^{soft} . This is in sharp contrast to the conclusion in Ref. [36] for high p_T single inclusive hadrons. To quantify the event-by-event correlation between the jet v_2^{jet} and the bulk hadron v_2^{soft} , we have fitted their correlation function from LBT simulations with a power-law ansatz and found a close to linear dependence of v_2^{jet} on v_2^{soft} . Such a linear correlation holds for different colliding energies, centrality classes and jet transverse momenta, and can be tested by more precise jet measurements in the future.

One of the special capabilities of the LBT model is to

explore signatures of jet-induced medium excitation in heavy-ion collisions which consists of recoil and “negative” partons, or Mach wave and diffusion wake, arising from jet-medium interaction. In this work, we found that jet-induced medium response which is influenced by the radial flow increases the jet elliptic anisotropy beyond the simple mechanism of length dependence of jet energy loss. Inclusion of the jet-induced medium response leads to a larger v_2^{jet} by 20~40% in the p_T range of 50~250 GeV/ c as compared to the case without medium response but with the same jet suppression factor R_{AA} by reducing the effective strong coupling constant. The enhancement of jet v_2^{jet} due to jet-induced medium response increases with the jet cone sizes. We also explored the effect of the shear viscosity of the bulk medium on the jet anisotropy which increases v_2^{jet} , but only slightly.

ACKNOWLEDGMENTS

We would like to thank Chi Ding for helpful discussions. This work is supported in part by Guangdong Major Project of Basic and Applied Basic Research No. 2020B0301030008, by National Natural Science Foundation of China (NSFC) under Grant Nos. 11935007, 11221504, 11861131009, 11890714, 12175122, 12075098 and 2021-867, by Science and Technology Program of Guangzhou No. 2019050001, by Fundamental Research Funds for Central Universities in China, by the Director, Office of Energy Research, Office of High Energy and Nuclear Physics, Division of Nuclear Physics, of the U.S. Department of Energy under Contract No. DE-AC02-05CH11231, by the US National Science Foundation under Grant No. ACI-1550228 within the JETSCAPE and OAC-2004571 within the X-SCAPE Collaboration, by EU ERDF and H2020 grant 82409, ERC grant ERC-2018-ADG-835105, Spanish AEI grant FPA2017-83814-P and MDM- 2016-0692, Xunta de Galicia Research Center accreditation 2019-2022. Computations in this study are performed at the NSC3/CCNU and the National Energy Research Scientific Computing Center (NERSC), a U.S. Department of Energy Office of Science User Facility located at Lawrence Berkeley National Laboratory and operated under Contract No. DE-AC02-05CH11231.

-
- [1] M. Gyulassy and M. Plumer, *Phys. Lett.* **B243**, 432 (1990).
 - [2] X.-N. Wang and M. Gyulassy, *Phys. Rev. Lett.* **68**, 1480 (1992).
 - [3] M. Gyulassy, I. Vitev, X.-N. Wang, and B.-W. Zhang, (2003), [arXiv:nucl-th/0302077](#).
 - [4] A. Majumder and M. Van Leeuwen, *Prog. Part. Nucl. Phys.* **66**, 41 (2011), [arXiv:1002.2206 \[hep-ph\]](#).
 - [5] Y. Mehtar-Tani, J. G. Milhano, and K. Tywoniuk, *Int. J. Mod. Phys. A* **28**, 1340013 (2013), [arXiv:1302.2579](#)

- [6] G.-Y. Qin and X.-N. Wang, *Int. J. Mod. Phys.* **E24**, 1530014 (2015), [arXiv:1511.00790 \[hep-ph\]](#).
- [7] S. Cao and X.-N. Wang, (2020), [arXiv:2002.04028 \[hep-ph\]](#).
- [8] R. Baier, Y. L. Dokshitzer, A. H. Mueller, S. Peigne, and D. Schiff, *Nucl. Phys.* **B483**, 291 (1997), [hep-ph/9607355](#).
- [9] R. Baier, Y. L. Dokshitzer, A. H. Mueller, S. Peigne, and D. Schiff, *Nucl. Phys.* **B484**, 265 (1997), [arXiv:hep-](#)

- ph/9608322 [hep-ph].
- [10] B. G. Zakharov, JETP Lett. **63**, 952 (1996), arXiv:hep-ph/9607440.
 - [11] M. Gyulassy, P. Levai, and I. Vitev, Nucl. Phys. **B594**, 371 (2001), arXiv:nucl-th/0006010.
 - [12] U. A. Wiedemann, Nucl. Phys. **A690**, 731 (2001), arXiv:hep-ph/0008241.
 - [13] X.-N. Wang and X.-F. Guo, Nucl. Phys. **A696**, 788 (2001), arXiv:hep-ph/0102230.
 - [14] P. Arnold, G. D. Moore, and L. G. Yaffe, JHEP **06**, 030 (2002), hep-ph/0204343.
 - [15] J. Casalderrey-Solana and X.-N. Wang, Phys. Rev. **C77**, 024902 (2008), arXiv:0705.1352 [hep-ph].
 - [16] Z.-T. Liang, X.-N. Wang, and J. Zhou, Phys. Rev. **D77**, 125010 (2008), arXiv:0801.0434 [hep-ph].
 - [17] Y.-Y. Zhang, G.-Y. Qin, and X.-N. Wang, Phys. Rev. **D100**, 074031 (2019), arXiv:1905.12699 [hep-ph].
 - [18] X.-F. Chen, C. Greiner, E. Wang, X.-N. Wang, and Z. Xu, Phys. Rev. **C81**, 064908 (2010), arXiv:1002.1165 [nucl-th].
 - [19] K. M. Burke *et al.* (JET), Phys. Rev. **C90**, 014909 (2014), arXiv:1312.5003 [nucl-th].
 - [20] .
 - [21] X. Feal, C. A. Salgado, and R. A. Vazquez, Phys. Lett. **B816**, 136251 (2021), arXiv:1911.01309 [hep-ph].
 - [22] S. Cao *et al.* (JETSCAPE), Phys. Rev. **C104**, 024905 (2021), arXiv:2102.11337 [nucl-th].
 - [23] X.-N. Wang, Phys. Rev. **C63**, 054902 (2001), arXiv:nucl-th/0009019 [nucl-th].
 - [24] J.-Y. Ollitrault, Phys. Rev. **D46**, 229 (1992).
 - [25] M. Gyulassy, I. Vitev, and X. N. Wang, Phys. Rev. Lett. **86**, 2537 (2001), arXiv:nucl-th/0012092 [nucl-th].
 - [26] M. Gyulassy, I. Vitev, X.-N. Wang, and P. Huovinen, Phys. Lett. **B526**, 301 (2002), arXiv:nucl-th/0109063.
 - [27] X.-N. Wang, Phys. Lett. **B595**, 165 (2004), arXiv:nucl-th/0305010.
 - [28] C. Shen, Nucl. Phys. **A1005**, 121788 (2021), arXiv:2001.11858 [nucl-th].
 - [29] U. Heinz and R. Snellings, Ann. Rev. Nucl. Part. Sci. **63**, 123 (2013), arXiv:1301.2826 [nucl-th].
 - [30] C. Gale, S. Jeon, and B. Schenke, Int. J. Mod. Phys. **A28**, 1340011 (2013), arXiv:1301.5893 [nucl-th].
 - [31] R. Derradi de Souza, T. Koide, and T. Kodama, Prog. Part. Nucl. Phys. **86**, 35 (2016), arXiv:1506.03863 [nucl-th].
 - [32] B. Betz, M. Gyulassy, and G. Torrieri, Phys. Rev. **C84**, 024913 (2011), arXiv:1102.5416 [nucl-th].
 - [33] D. Zigic, I. Salom, J. Auvinen, M. Djordjevic, and M. Djordjevic, Phys. Lett. **B791**, 236 (2019), arXiv:1805.04786 [nucl-th].
 - [34] D. Zigic, B. Ilic, M. Djordjevic, and M. Djordjevic, Phys. Rev. **C101**, 064909 (2020), arXiv:1908.11866 [hep-ph].
 - [35] C. Andres, N. Armesto, H. Niemi, R. Paatelainen, and C. A. Salgado, Phys. Lett. **B803**, 135318 (2020), arXiv:1902.03231 [hep-ph].
 - [36] J. Noronha-Hostler, B. Betz, J. Noronha, and M. Gyulassy, Phys. Rev. Lett. **116**, 252301 (2016), arXiv:1602.03788 [nucl-th].
 - [37] J. Xu, J. Liao, and M. Gyulassy, Chin. Phys. Lett. **32**, 9 (2015), arXiv:1411.3673 [hep-ph].
 - [38] J. Xu, J. Liao, and M. Gyulassy, JHEP **02**, 169 (2016), arXiv:1508.00552 [hep-ph].
 - [39] S. Shi, J. Liao, and M. Gyulassy, Chin. Phys. **C43**, 044101 (2019), arXiv:1808.05461 [hep-ph].
 - [40] R. J. Fries, B. Muller, C. Nonaka, and S. A. Bass, Phys. Rev. Lett. **90**, 202303 (2003), arXiv:nucl-th/0301087 [nucl-th].
 - [41] R. J. Fries, B. Muller, C. Nonaka, and S. A. Bass, Phys. Rev. **C68**, 044902 (2003), nucl-th/0306027.
 - [42] V. Greco, C. M. Ko, and P. Levai, Phys. Rev. Lett. **90**, 202302 (2003), arXiv:nucl-th/0301093 [nucl-th].
 - [43] V. Greco, C. M. Ko, and P. Levai, Phys. Rev. **C68**, 034904 (2003), nucl-th/0305024.
 - [44] V. Greco, C. M. Ko, and R. Rapp, Phys. Lett. **B595**, 202 (2004), nucl-th/0312100.
 - [45] D. Molnar and S. A. Voloshin, Phys. Rev. Lett. **91**, 092301 (2003), nucl-th/0302014.
 - [46] C. B. Chiu, R. C. Hwa, and C. Yang, Phys. Rev. **C78**, 044903 (2008), arXiv:0801.2183 [nucl-th].
 - [47] R. C. Hwa and C. Yang, Phys. Rev. Lett. **93**, 082302 (2004), arXiv:nucl-th/0403001.
 - [48] W. Zhao, C. M. Ko, Y.-X. Liu, G.-Y. Qin, and H. Song, Phys. Rev. Lett. **125**, 072301 (2020), arXiv:1911.00826 [nucl-th].
 - [49] S. Cao, Nucl. Phys. **A1005**, 121984 (2021).
 - [50] X. Dong, Y.-J. Lee, and R. Rapp, Ann. Rev. Nucl. Part. Sci. **69**, 417 (2019), arXiv:1903.07709 [nucl-ex].
 - [51] W.-J. Xing, S. Cao, G.-Y. Qin, and H. Xing, Phys. Lett. **B805**, 135424 (2020), arXiv:1906.00413 [hep-ph].
 - [52] W. Zhao, W. Ke, W. Chen, T. Luo, and X.-N. Wang, Phys. Rev. Lett. **128**, 022302 (2022), arXiv:2103.14657 [hep-ph].
 - [53] S. D. Ellis, Z. Kunszt, and D. E. Soper, Phys. Rev. Lett. **64**, 2121 (1990).
 - [54] X.-N. Wang and Y. Zhu, Phys. Rev. Lett. **111**, 062301 (2013), arXiv:1302.5874 [hep-ph].
 - [55] Y. He, T. Luo, X.-N. Wang, and Y. Zhu, Phys. Rev. **C91**, 054908 (2015), arXiv:1503.03313 [nucl-th].
 - [56] S. Cao, T. Luo, G.-Y. Qin, and X.-N. Wang, Phys. Rev. **C94**, 014909 (2016), arXiv:1605.06447 [nucl-th].
 - [57] L.-G. Pang, Y. Hatta, X.-N. Wang, and B.-W. Xiao, Phys. Rev. **D91**, 074027 (2015), arXiv:1411.7767 [hep-ph].
 - [58] L. Pang, Q. Wang, and X.-N. Wang, Phys. Rev. **C86**, 024911 (2012), arXiv:1205.5019 [nucl-th].
 - [59] L.-G. Pang, H. Petersen, and X.-N. Wang, Phys. Rev. **C97**, 064918 (2018), arXiv:1802.04449 [nucl-th].
 - [60] Y. He, S. Cao, W. Chen, T. Luo, L.-G. Pang, and X.-N. Wang, Phys. Rev. **C99**, 054911 (2019), arXiv:1809.02525 [nucl-th].
 - [61] T. Luo, S. Cao, Y. He, and X.-N. Wang, Phys. Lett. **B782**, 707 (2018), arXiv:1803.06785 [hep-ph].
 - [62] S.-L. Zhang, T. Luo, X.-N. Wang, and B.-W. Zhang, Phys. Rev. **C98**, 021901 (2018), arXiv:1804.11041 [nucl-th].
 - [63] X.-F. Guo and X.-N. Wang, Phys. Rev. Lett. **85**, 3591 (2000), arXiv:hep-ph/0005044.
 - [64] A. Majumder, Phys. Rev. **D85**, 014023 (2012), arXiv:0912.2987 [nucl-th].
 - [65] B.-W. Zhang, E. Wang, and X.-N. Wang, Phys. Rev. Lett. **93**, 072301 (2004), arXiv:nucl-th/0309040 [nucl-th].
 - [66] W. Chen, S. Cao, T. Luo, L.-G. Pang, and X.-N. Wang, Phys. Lett. **B777**, 86 (2018), arXiv:1704.03648 [nucl-th].
 - [67] W. Chen, S. Cao, T. Luo, L.-G. Pang, and X.-N. Wang, Phys. Lett. **B810**, 135783 (2020), arXiv:2005.09678 [hep-ph].
 - [68] Z. Yang, W. Chen, Y. He, W. Ke, L. Pang, and X.-N. Wang, (2021), arXiv:2101.05422 [hep-ph].

- [69] A. Kurganov and E. Tadmor, Numerical Methods for Partial Differential Equations **18**, 584 (2002).
- [70] Z.-W. Lin, C. M. Ko, B.-A. Li, B. Zhang, and S. Pal, *Phys. Rev.* **C72**, 064901 (2005), [arXiv:nucl-th/0411110 \[nucl-th\]](#).
- [71] P. Huovinen and P. Petreczky, *Nucl. Phys.* **A837**, 26 (2010), [arXiv:0912.2541 \[hep-ph\]](#).
- [72] X.-N. Wang and M. Gyulassy, *Phys. Rev.* **D44**, 3501 (1991).
- [73] M. Gyulassy and X.-N. Wang, *Comput. Phys. Commun.* **83**, 307 (1994), [arXiv:nucl-th/9502021](#).
- [74] G. Aad *et al.* (ATLAS), *JHEP* **11**, 183 (2013), [arXiv:1305.2942 \[hep-ex\]](#).
- [75] A. M. Sirunyan *et al.* (CMS), *Phys. Lett. B* **789**, 643 (2019), [arXiv:1711.05594 \[nucl-ex\]](#).
- [76] M. Cacciari, G. P. Salam, and G. Soyez, *Eur. Phys. J.* **C72**, 1896 (2012), [arXiv:1111.6097 \[hep-ph\]](#).
- [77] G. Aad *et al.* (ATLAS), *Phys. Lett. B* **719**, 220 (2013), [arXiv:1208.1967 \[hep-ex\]](#).
- [78] G. Aad *et al.* (ATLAS), *Phys. Rev. Lett.* **111**, 152301 (2013), [arXiv:1306.6469 \[hep-ex\]](#).
- [79] A.-C.-. ATLAS (ATLAS), (2020).
- [80] C. Loizides and A. Morsch, *Phys. Lett. B* **773**, 408 (2017), [arXiv:1705.08856 \[nucl-ex\]](#).
- [81] A. Huss, A. Kurkela, A. Mazeliauskas, R. Paatelainen, W. van der Schee, and U. A. Wiedemann, *Phys. Rev. Lett.* **126**, 192301 (2021), [arXiv:2007.13754 \[hep-ph\]](#).
- [82] M. Xie, X.-N. Wang, and H.-Z. Zhang, *Phys. Rev. C* **103**, 034911 (2021), [arXiv:2003.02441 \[hep-ph\]](#).
- [83] S. Cao, L.-G. Pang, T. Luo, Y. He, G.-Y. Qin, and X.-N. Wang, *Proceedings, 8th International Conference on Hard and Electromagnetic Probes of High-energy Nuclear Collisions: Hard Probes 2016 (HP2016): Wuhan, Hubei, China, September 23-27, 2016*, *Nucl. Part. Phys. Proc.* **289-290**, 217 (2017).
- [84] E. Abbas *et al.* (ALICE), *Phys. Lett. B* **726**, 610 (2013), [arXiv:1304.0347 \[nucl-ex\]](#).
- [85] J. Adam *et al.* (ALICE), *Phys. Lett. B* **772**, 567 (2017), [arXiv:1612.08966 \[nucl-ex\]](#).
- [86] M. Aaboud *et al.* (ATLAS), *Phys. Lett. B* **790**, 108 (2019), [arXiv:1805.05635 \[nucl-ex\]](#).
- [87] B. Schenke, C. Gale, and S. Jeon, *Phys. Rev.* **C80**, 054913 (2009), [arXiv:0909.2037 \[hep-ph\]](#).
- [88] C. Park, S. Jeon, and C. Gale, *Proceedings, 27th International Conference on Ultrarelativistic Nucleus-Nucleus Collisions (Quark Matter 2018): Venice, Italy, May 14-19, 2018*, *Nucl. Phys.* **A982**, 643 (2019), [arXiv:1807.06550 \[nucl-th\]](#).
- [89] K. C. Zapp, F. Krauss, and U. A. Wiedemann, *JHEP* **03**, 080 (2013), [arXiv:1212.1599 \[hep-ph\]](#).
- [90] K. C. Zapp, *Eur. Phys. J.* **C74**, 2762 (2014), [arXiv:1311.0048 \[hep-ph\]](#).
- [91] J. Casalderrey-Solana, D. C. Gulhan, J. G. Milhano, D. Pablos, and K. Rajagopal, *JHEP* **10**, 019 (2014), [Erratum: *JHEP*09,175(2015)], [arXiv:1405.3864 \[hep-ph\]](#).
- [92] Z. Hulcher, D. Pablos, and K. Rajagopal, *JHEP* **03**, 010 (2018), [arXiv:1707.05245 \[hep-ph\]](#).
- [93] Y. Tachibana, N.-B. Chang, and G.-Y. Qin, *Phys. Rev.* **C95**, 044909 (2017), [arXiv:1701.07951 \[nucl-th\]](#).